The Canadian Journal of Chemical Engineering

formerly

CANADIAN JOURNAL OF TECHNOLOGY

CONTENTS

Studies of Bubble Formation and Rise	*A. A. Poutanen* *A. I. Johnson*	**93**
Kinetics of the Vapor-Phase Oxidation of Napthalene over a Vanadium Catalyst	*K. A. Shelstad* *J. Downie* *W. F. Graydon*	**102**
Oxidation of Ethylene Using Silver Catalyst Coated Strips in an Inert Fluidized Bed	*E. Echigoya* *G. L. Osberg*	**108**
Evaporation Rates in Spray Drying	*J. Dlouhy* *W. H. Gauvin*	**113**
Letters to the Editor	*L. W. Shemilt* *James C. M. Li* *Benjamin C.-Y. Lu*	**121**
Industrial Section		
Effect of Diesel Locomotive Operation on Atmospheric Conditions in a Railway Tunnel	*R. P. Rennie* *Z. Jegier* *Morris Katz*	**123**

Published by
THE CHEMICAL INSTITUTE OF CANADA
OTTAWA CANADA

Photograph taken at C-I-L Central Research Laboratory, McMasterville, Que.

POLYMERIC PRECISION

This is an ebulliometer—being assembled by the master glass-blower on his own lathe at our Central Research Laboratory.

The ebulliometer uses two vapor lift pumps such as those found in electric coffee percolators. One circulates a polymer solution while the other circulates boiling solvent—each liquid stream is directed over a temperature detector so sensitive that a difference of one-millionth of 1°C. may be sensed. This device allows the measurement of high molecular weights related to the physical properties of polymers.

Such C-I-L research contributes to higher standards of performance in the plastics industry . . . to new and better plastic products . . . and—through better technical service—to greater success in the application of these new materials to modern living.

C-I-L **CANADIAN INDUSTRIES LIMITED**

Serving Canadians Through Chemistry

Agricultural Chemicals • Ammunition • Coated Fabrics • Industrial Chemicals • Commercial Explosives • Paints • Plastics • Textile Fibres

The Canadian Journal of Chemical Engineering

formerly

Canadian Journal of Technology

published by

The Chemical Institute of Canada

VOLUME 38 AUGUST, 1960 NUMBER 4

Authorized as second class mail, Post Office Department, Ottawa. Printed in Canada

Manuscripts for publication should be submitted to the Editor: Dr. A. Cholette, Faculty of Science, Laval University, Boulevard de l'Entente, Quebec, Que. (Instructions to authors are on the next page).

Editorial, Production and Circulation Offices: 48 Rideau Street, Ottawa 2, Ont.

Advertising Office: C. N. McCuaig, manager of advertising sales, *The Canadian Journal of Chemical Engineering*, Room 601, 217 Bay Street, Toronto, Ont. Telephone—EMpire 3-3871.

Plates and Advertising Copy: Send to *The Canadian Journal of Chemical Engineering*, 48 Rideau Street, Ottawa 2, Ont.

Subscription Rates: In Canada—$6.00 per year and $1.25 per single copy; U.S. and U.K.—$7.00, Foreign—$7.50.

Change of Address: Advise Circulation Department in advance of change of address, providing old as well as new address. Enclose address label if possible.

The Canadian Journal of Chemical Engineering is published by The Chemical Institute of Canada every two months.

The Canadian Journal of Chemical Engineering

INSTRUCTIONS TO AUTHORS

Manuscript Requirements for Articles

1. The manuscript should be in English or French.
2. The original and two copies of the manuscript should be supplied. These are to be on 8½ x 11 inch sheets, typewritten, and double spaced. Each page should be numbered.
3. Symbols should conform to American Standards Association. An abridged set of acceptable symbols is found in the third edition of Perry's Chemical Engineers' Handbook. Greek letters and subscripts and superscripts should be carefully made.
4. Abstracts of not more than 200 words in English indicating the scope of the work and the principal findings should accompany all technical papers.
5. References should be listed in the order in which they occur in the paper, after the text, using the form shown here: "Othmer, D. F., Jacobs, Jr., J. J., and Levy, J. F., Ind. Eng. Chem. **34**, 286 (1942). Abbreviations of journal names should conform to the "List of Periodicals Abstracted by Chemical Abstracts". Abbreviations of the common journals are to be found in Perry's Handbook also. All references should be carefully checked with the original article.
6. Tables should be numbered in Arabic numerals. They should have brief descriptive titles and should be appended to the paper. Column headings should be brief. Tables should contain a minimum of descriptive material.
7. All figures should be numbered from 1 up, in Arabic numerals. Drawings should be carefully made with India ink on white drawing paper or tracing linen. All lines should be of sufficient thickness to reproduce well, especially if the figure is to be reduced. Letters and numerals should be carefully and neatly made, with a stencil. Generally speaking, originals should not be more than twice the size of the desired reproduction; final engravings being 3¼ in. or 7 in. wide depending on whether one column or two is used.
8. Photographs should be made on glossy paper with strong contrasts. Photographs or groups of photographs should not be larger than three times the size of the desired reproduction.
9. All tables and figures should be referred to in the text.

Submission of Manuscripts

1. The three copies of the manuscript, including figures and tables, should be sent directly to:
   DR. A. CHOLETTE, editor,
   The Canadian Journal of Chemical Engineering,
   Faculty of Science, Laval University,
   Boulevard de l'Entente,
   Quebec, Que.
2. The authors addresses and titles should be submitted with the manuscript.
3. The author may suggest names of reviewers for his article, but the selection of the reviewers will be the responsibility of the editor. Each paper or article is to be reviewed by two chemical engineers familiar with the topic. Reviewers will remain anonymous.
4. All correspondence regarding reviews should be directed to the editor.

Reprints

1. At least 50 free "tear sheets" of each paper will be supplied.
2. Additional reprints may be purchased at cost. An estimated cost of reprints, with an attached order form, will be sent to the author with the galley proofs.
3. Orders for reprints must be made before the paper has appeared in the Journal.

Communications, Letters and Notes to the Editor

Short papers, as described below, will be considered for publication in this Journal. Their total length should not exceed 600 words, or its equivalent.

Communications

A communication is a prompt preliminary report of observations made which are judged to be sufficiently important to warrant expedited publication. It usually calls for a more expanded paper in which the original matter is republished with more details.

Letters

A letter consists of comments or remarks submitted by readers or authors in connection with previously published material. It may deal with various forms of discussion arising out of a publication or it may simply report and correct inadvertent errors.

Notes

A note is a short paper which describes a piece of work not sufficiently important or complete to make it worth a full article. It may refer to a study or piece of research which, while it is not finished and may not be finished, offers interesting aspects or facts. As in the case of an article a note is a final publication.

* * *

Studies of Bubble Formation and Rise[1]

A. A. POUTANEN[2] *and A. I. JOHNSON*[3]

Preliminary to mass transfer studies, studies of bubble shape and area during formation and of velocity of rise after formation were made for nitrogen bubbles in water and two hydrocarbon oils.

Bubble profiles were found to fit an empirical equation of the form $r^n\theta = 1$ where r and θ are polar coordinates.

Quantative studies of bubble volume and area as a function of time are reported.

A limited correlation for the velocity of rise of a chain of bubbles in a viscous oil is presented.

Introduction

(a) Bubble Shape

In any study of mass transfer from bubbles or drops, interfacial area is of prime importance. During bubble rise this area can be evaluated quite readily, but during bubble formation at a nozzle the area varies in some manner with time. For an effective study of transfer during formation this area must be known.

In most studies of mass transfer during formation, the assumption has been made that the volume of the bubble grows constantly with time and the surface area is computed assuming the bubble to be spherical at all times. However, any sequence of pictures taken during bubble formation reveals that the bubble is not entirely spherical. Especially during the break-off period the bubble has an elongated neck by which it is attached to the nozzle.

For the calculation of either surface area or volume of a bubble at a nozzle, some knowledge of the shape is necessary. For a stationary bubble or a pendant drop, the shape had been established theoretically by Bashforth and Adams[1] who balanced pressure forces inside and outside the surface. The final equation could not be solved exactly; instead, using a numerical method Bashforth and Adams prepared tables from which the shape could be drawn. They also derived an equation for the volume of the bubble above a given horizontal plane by balancing surface tension forces against weight and pressure forces. Tables which were quite accurate but only for a limited range, were prepared.

The theory given by Bashforth and Adams was used mainly to calculate boundary tension by means of pendant drops. Early workers, such as Worthington[2] and Ferguson[3] found difficulties in solving similar equations using the measurements they made. Not until Andreas, Hauser, and Tucker[4] reviewed and simplified the method for finding boundary tension was any degree of accuracy attainable. Later Fordham[5] solidified thei findings and prepared extensive tables.

The work by Siemes[6], Lane and Green[7], Wark[8], and Freud and Harkins[9] gave a good summary of bubble shape and volume as predicted by Bashforth and Adams. Several of these papers, notably Siemes, discussed solutions of the equations, all being of an approximate nature.

It must be stressed here that the equations of Bashforth and Adams were for a stationary bubble or a pendant drop. For a growing bubble dynamic forces would have to be considered for a theoretical solution and, as yet, no work of this nature has been done.

A less exact method of finding drop volume and shape was proposed by Null and Johnson[10] from direct observation of the shape.

(b) Bubble Velocity

Another important factor in mass transfer work is the magnitude of the time of contact, normally calculated from the height of rise and the bubble velocity. In surveying literature one finds any amount of data on the rise of single bubbles in various liquids. However, little information is obtainable on the rise of a stream of bubbles that could occur in a study of mass transfer.

The rise of single air bubbles through different fluids of widely varying physical properties was studied by Haberman and Morton[11], Garner and Hammerton[12], Peebles and Garber[13], O'brien and Gosline[14], Robinson[15], Datta, Napier, and Newitt[16] and many others. These studies covered the range of Reynolds numbers from 10^{-5} to 3000. For lower Reynolds numbers, i.e. $N_{Re} \simeq 2$, agreement was found with Stokes' law[17] and the theory put forth by Hadamard[18] and Rybczynski[19].

The theory of Hadamard-Rybczynski predicted a 50% increase in the velocity of a gas bubble in a liquid if circulation existed inside the bubble. Bond and Newton[20] proposed a relationship for the critical radius at which transition from a rigid to a circulating sphere occurred. Garner and Hammerton disgreed with this proposed criterion and presented data for numerous systems showing the experimental transition radii. However, they did not have enough data for a correlation.

Haberman and Morton studied the rise of single air bubbles in various liquids and also found a transition from stagnation to circulation inside of the bubbles. The drag curves of the bubbles fell between the two limiting curves, i.e. the drag curves of rigid and fluid spheres. No correlation was obtained for the transition radii.

Any velocity data reported for a stream of bubbles had shown an increase in velocity compared to that of a single bubble. Haberman and Morton found that for a mineral oil with a viscosity of 58 c.p. and a density of 0.866 gm/cc., increases

[1]*Manuscript received February 8; accepted April 25, 1960.*
[2]*Nylon Intermediates Works, Du Pont of Canada Limited, Maitland, Ont.*
[3]*Associate Professor of Chemical Engineering, University of Toronto, Toronto, Ont.*
Contribution from the Department of Chemical Engineering, University of Toronto, Toronto, Ont.

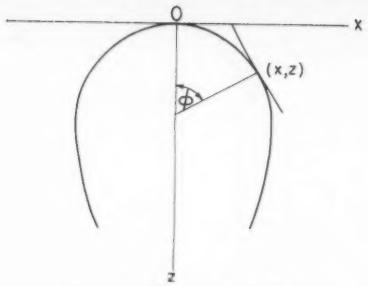

$$\frac{1}{\rho} + \frac{\sin\phi}{x} = \frac{2}{b} + \frac{\beta z}{b^2}$$

Figure 1—Theoretical bubble shape.

in velocity of 9 and 39% were obtained for a bubble diameter of 0.34 cm. with the bubbles 7.7 cm. and 3.2 cm. apart respectively.

Garner and Hammerton also found an increase in velocity. For a white oil (viscosity of 198 centistokes at 20°C.) velocities 2.5 times that calculated from Stokes' law were obtained at frequencies higher than 3 bubbles per second.

At a frequency of one bubble per second, Coppock and Meiklejohn[21] found an increase of 30% in velocity of air bubbles in water for a diameter of 0.2 cm. As the bubble diameter increased, the difference in velocity between single and multiple bubbles decreased and became the same at a diameter of 0.6 cm.

Garner and Hammerton stated that Guyer and Pfister[22] found increases of 12 to 50% in velocity for carbon dioxide bubbles in water at a frequency of 3 bubbles per second.

Other workers[23,14,16] observed increases in velocity over that of single bubbles, but no systematic study of the effect of bubble frequency, column size, and seal height on bubble velocity has been made. In any mass transfer work a single bubble would be more difficult to analyse than a stream of bubbles and with the latter it would be imperative to know the velocity of rise in order to calculate a time of contact.

Theoretical Discussion

(a) Bubble Shape

A good summary of bubble or pendant drop shape as derived by Bashforth and Adams is given by Wark[8]. For a stationary bubble attached to a nozzle and at equilibrium in the liquid the theoretical shape is

$$\frac{1}{\rho} + \frac{\sin\phi}{x} = \frac{2}{b} + \frac{\beta z}{b^2} \quad \ldots\ldots(1)$$

where ρ and $x/\sin\phi$ are the two principle radii of curvature at point (x, z), b is the radius of curvature at point O, and $\beta = \frac{b^2 g(\rho_G - \rho_L)}{\sigma}$. The gas and liquid densities are ρ_G and ρ_L respectively, the surface tension is σ, and the acceleration due to gravity is g. The x and z axes are located as shown in Figure 1. Solutions of this equation can be found in the work of Bashforth and Adams, and lately extended by Fordham.

The volume, V, above a given horizontal plane was also derived and the final equation is

$$V = \frac{\pi x^2 b^2}{\beta}\left(\frac{1}{\rho} - \frac{\sin\phi}{x}\right) \quad \ldots\ldots(2)$$

Bashforth and Adams also solved this equation but only over a limited range.

Null and Johnson proposed a different, less exact, method for finding volumes of drops. They assumed the bubble to be composed of two parts, a sphere placed on a right-truncated cone passing through the circumference of the nozzle. The bubble shape did not lend itself too accurately to this treatment.

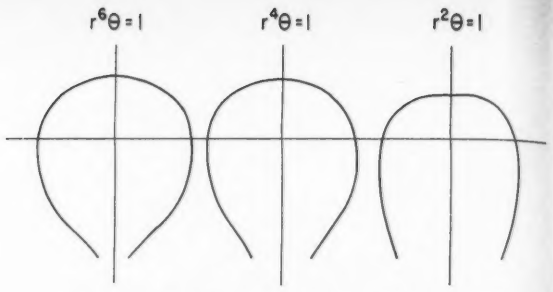

Figure 2—Various bubble shapes for proposed Equation $r^n\theta = 1$.

In this work a new, empirical, and somewhat simplified equation for bubble shape is proposed. It was found that part of a lituus, $r^2\theta = 1$, closely approximated a bubble shape. By introducing a variable power, n, in place of the power 2, the equation could be used for different bubble shapes as in Figure 2. The resulting equation is

$$r^n\theta = 1 \quad \ldots\ldots(3)$$

where r and θ are in polar coordinates.

For the surface area and volume Equation (3), from $\theta = 0$ to π, is revolved about the polar axis.

$$\text{Area} = 2\pi \int_{\theta_1}^{\pi} \frac{\sin\theta}{\theta^{2/n}} \sqrt{1 + \frac{1}{n^2\theta^2}}\, d\theta \quad \ldots\ldots(4)$$

$$\text{Volume} = -\pi \int_{\theta_1}^{\pi} \frac{\sin^3\theta}{\theta^{3/n}} \left(1 + \frac{1}{n\,\theta\tan\theta}\right) d\theta \quad \ldots\ldots(5)$$

These equations were solved by numerical integration using an I.B.M. 650 computer. Table* 2 and 3 filed with the American Documentation Institute No. 6343 permit estimation of surfaces and volumes of revolution; in these tables the angles are reported in degrees rather than in radians.

(b) Bubble Velocity

For a single bubble rising in an infinite medium of high viscosity with inertia forces small compared to viscous forces, Stokes' law will hold. The resistance to the motion of the bubble will be

$$F = 6\pi\mu r v \quad \ldots\ldots(6)$$

where μ is the viscosity, r the radius, and v the velocity. A mathematical treatment can be found in Lamb's "Hydrodynamics"[24]. Equating buoyant force of the bubble against the resistance to motion results in

$$v = \frac{2}{9}\left(\frac{\rho_L - \rho_G}{\mu}\right) g r^2 \quad \ldots\ldots(7)$$

or, if $\rho_L >> \rho_G$

$$v = \frac{2}{9}\frac{g r^2}{\nu} \quad \ldots\ldots(8)$$

where ν is the kinematic viscosity. Equation (8), applicable to a gas bubble, is known as Stokes' law, and it holds for bubble

*Tables 2 and 3 of this paper have been deposited as Document No. 6343 with the ADI Auxiliary Publications Project, Photoduplication Service, Library of Congress, Washington 25, D.C. A copy may be obtained by citing the Document No. and by remitting $1.25 for photoprints, or $1.25 for 35 mm. microfilm. Advance payment is required. Make cheques or money orders payable to: Chief, Photoduplication Service, Library of Congress.

Reynolds numbers below 2 if the bubble behaves as a rigid sphere with no slip at the surface.

The motion of fluid spheres was studied independently by Hadamard[18] and Rybczynski[19]. They found a variation in the resistance to motion if any circulation existed inside of the sphere. The derivation is also given by Lamb. This resistance is formulated as

$$F = 6\pi\mu r v k \quad \ldots\ldots (9)$$

$$\text{where } k = \frac{2\mu + 3\mu_i}{3\mu + 3\mu_i} \quad \ldots\ldots (10)$$

where μ is the viscosity of the continuous phase and μ_i the viscosity inside the bubble. Since liquid viscosity is much greater than that of a gas, Equation (9) becomes

$$F = 4\pi\mu r v \quad \ldots\ldots (11)$$

and the velocity

$$v = \frac{1}{3}\frac{gr^2}{\nu} \quad \ldots\ldots (12)$$

This is a 50% increase compared to Stokes' law, Equation (8).

Scope of This Work

The purpose of this work was threefold: to obtain data on the variation of bubble surface area and volume during formation, to find the actual formation time, and to obtain velocity data for the systems used.

Using 16mm. movie film, photographs were taken of bubbles forming at a nozzle. From the projected bubble tracing measurements were taken and the area and volume were calculated using an equation approximating the bubble shape. Also, from these films the actual formation time for various bubble diameters was observed.

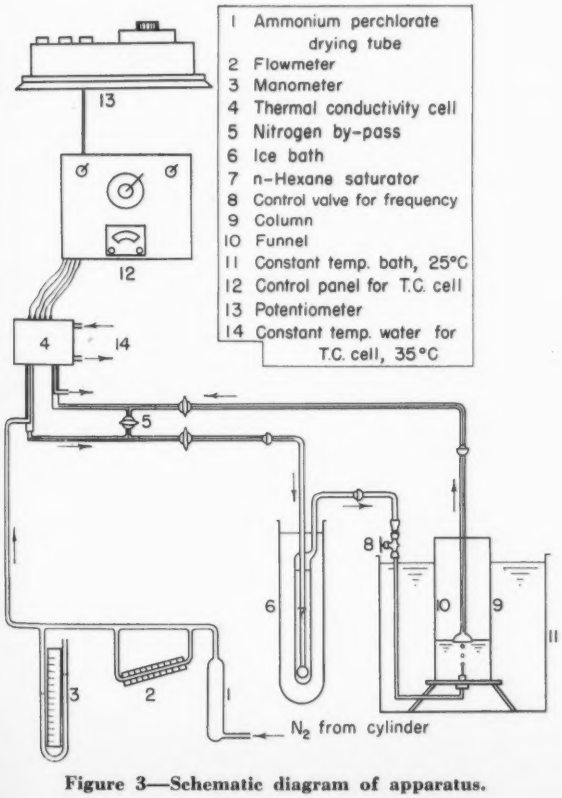

Figure 3—Schematic diagram of apparatus.

The velocity of rise was measured using two different methods which will be discussed later in more detail.

The systems studied corresponded to the mass transfer runs, i.e. a nitrogen bubble containing n-hexane vapor was passed through Paraffinol, a heavy mineral oil, and also through a light mineral oil. Some bubble shapes for air in water are included.

Apparatus

The apparatus used for photographing bubble shapes during formation is shown in Figure 3. The inlet nitrogen stream from a cylinder (Linde Company) was passed through a magnesium perchlorate drying tube into the flowmeter which measured the volume flow at the pressure of the gas. The dry nitrogen, after passing through the thermal conductivity cell, was directed through a saturator containing n-hexane at 0°C. The saturated stream then formed bubbles in the continuous phase of Paraffinol, a heavy mineral oil. At the desired bubble frequency and diameter, movies were taken using a 16 mm. Fastax camera (Wollensak Optical Company, Rochester, N.Y.). Dupont 930A reversal type film was used at a speed of 1000 frames per second. The lighting consisted of a single No. 2 photoflood placed directly behind the column, with a translucent plastic sheet to diffuse the light into an even background.

It was found that only one nozzle, inside diameter of 0.059 cm., was necessary to produce a 50% increase in bubble diameter from about 0.3 to 0.45 cm.

The apparatus used for determining bubble rise velocity was the same as that in the mass transfer runs since the data were recorded with the transfer data. To measure the distance between successive bubbles, two techniques were employed, movie and still film, and a cathetometer (Gaertner Scientific Corporation, Chicago, U.S.A.) and stroboscopic light. The frequency data were obtained from a strobotac (Model 631-B, General Radio Company, Cambridge, Mass.).

It was necessary to have two reference marks available for the film technique. A ⅛″ brass rod set into a circular ⅛″ thick, 1″ diameter brass plate was made. The rod had three marks approximately 2 cm. apart. The complete piece fitted into the nozzle assembly.

Physical properties of the materials employed are listed in Table 1.

TABLE 1

Normal Hexane	
Refractive index, n_D 25°C.	1.3712
Density, gm./cc. at 20°C.	0.65813
"Paraffinol", Heavy Mineral Oil	
Gravity °API	28.0
Specific gravity 60/60°F.	0.8871
Refractive index, n_D 20°C.	1.4812
Viscosity, SUS 100°F.	356.9
Viscosity, SUS 210°F.	52.62
Viscosity index	72.7
Characterization value	12.35
Average molecular weight	425
Composition: Weight per cent	
Aromatics	1
Naphthenes	38
Paraffins	61
Light Oil	
Gravity °API	37.1
Specific gravity 60/60 °F.	0.8393
Viscosity, SUS 100°F.	70.3
Viscosity, SUS 210°F.	36.2
Viscosity index	111
Mean average boiling point °F.	705
Average molecular weight	320

Procedure

(a) Area and Volume

In starting up the equipment the flow rate was set to approximately the desired flow and then the continuous phase was added to the column. This precaution was necessary to prevent any leakage into the nozzle. After the addition of the oil the flow rate and frequency were adjusted to give the bubble diameter needed. A small valve just before entry of the gas into the column served as a good regulator for the frequency. The apparatus was then operated until flow rate and frequency fluctuations had disappeared. With 50 feet of film in the camera, movies were taken of bubbles forming at the nozzle.

Five bubble diameters from 0.3 to 0.45 cm. were studied.

(b) Velocity of Rise

Knowing the frequency and distance between successive bubbles, the velocity of rise can be calculated. This distance was determined in two ways.

As each bubble moved up the column it was illuminated by the light from the strobotac. When the strobotac and bubble frequencies were the same, the illuminated bubbles seemed to remain in one place. Actually each bubble moved successively from one lighted position to another as the strobotac flashed. Using the cathetometer the distance between these lighted bubbles was measured.

Any fluctuation in frequency of either the bubbles or the light made it difficult to obtain a stationary image. For this reason the distance between bubbles was measured photographically. Both 35 mm. still and 16 mm. movie film were taken. Projecting the film onto a screen allowed the distance to be calculated using the two reference marks.

It should be pointed out that neither the acceleration nor the terminal velocities of the bubbles have been measured in this study.

Discussion of Results

(a) Bubble Shapes During Formation

From the 16 mm. film bubble, outlines were traced at various times during formation, by projecting the film onto graph paper. Only a section of film having a complete bubble growth and release was considered. The time for the various shapes was calculated from light "blips" exposed on the edge of the film during running operation at a rate of 120 per second. The sequence of pictures in Figure 4 shows the bubble shapes for the system, Paraffinol-n-hexane-nitrogen for a final bubble diameter of 0.375 cm.

Since a small nozzle was used, the bubble shape was quite spherical. As the bubble started forming it had a flattened appearance of an oblate spheroid and this was prevalent with all of the bubble diameters studied.

Figure 5 shows bubble shapes for a nitrogen bubble forming in water. The shapes here differed from those of Figure 4 in that the neck of the bubble is larger and more elongated. Surface tension and nozzle size caused these differences. As will be shown later the area variation during formation depends altogether on the bubble shape.

In Figures 4 and 5, values using Equation (3) were also plotted to show the comparison of the actual to the predicted shape.

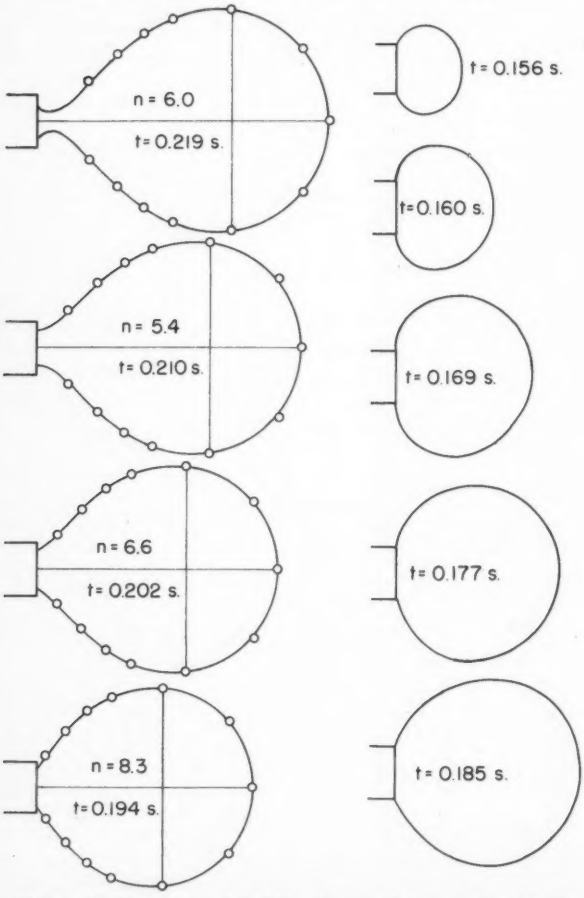

Figure 4—Sequence of bubble shapes. System: Paraffinal-n-Hexane-Nitrogen; Orifice diameter = 0.059 cm.; o — Equation 3; Final d = 0.370 cm.

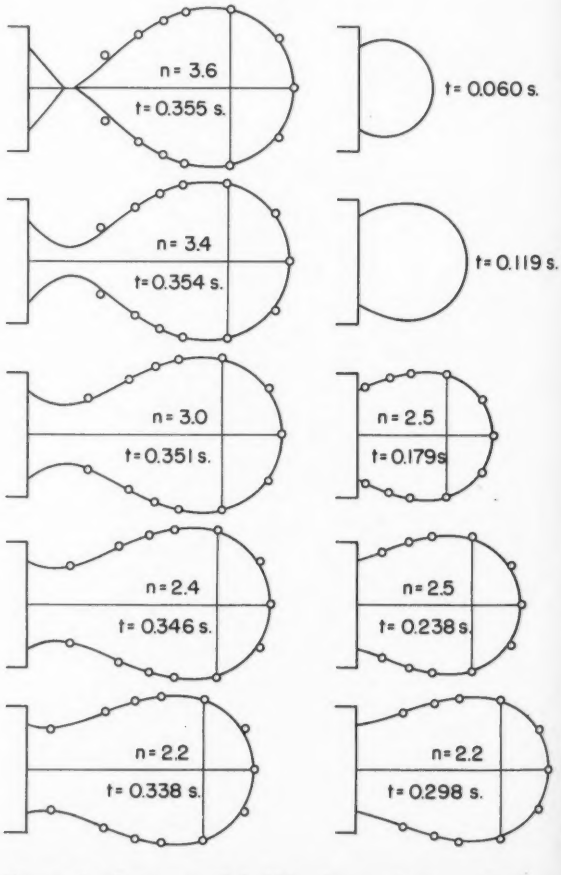

Figure 5—Sequence of bubble shapes. System: Water — Nitrogen; Orifice diameter = 0.206 cm.; o — Equation 3; Final d = 0.424 cm.

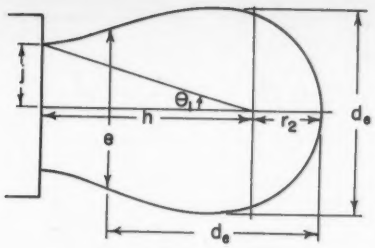

Ratio $\frac{e}{d_e} = s = 0.808$
$n = 2.1$
Outside diameter of nozzle = 0.308 cm.

Figure 6—Sample calculation of surface area and volume.

(b) Sample Calculation of Area and Volume

Referring to Figure 6 of a tracing of the bubble outline, the ratio $e/d_e = s$ was determined. Andreas, Hauser, and Tucker[4] proposed this same ratio as a shape factor for pendant drops. The values of n for Equation (3) were calculated for each corresponding s ratio. (Figure 7)

As a reference measurement the outside diameter of the nozzle was used except when the smallest nozzle (d_i = 0.059 cm.) was in the column. For the latter case greater accuracy was obtained using a 4 mm. O.D. cylinder, 4 mm. high, which fitted over the nozzle leaving 2 mm. of the tip exposed.

A sample calculation for one bubble shape, a nitrogen bubble in water, Figure 6, was as follows:

Ratio $e/d_e = s$	= 0.808
n value (Figure 7)	= 2.14
Actual outside diameter of nozzle	= 0.308 cm.
Outside diameter of nozzle measured on tracing	= 42 units
Maximum bubble width, d_e, on tracing	= 47 units
Actual bubble width = 47/42 × 0.308	= 0.345 cm.
Dimensionless bubble width, d', for Equation (3) (Figure 7 for n = 2.14)	= 1.715
Conversion, d/d', factor to change dimensionless units to actual length = 0.345/1.715	= 0.201 cm.
Angle θ_1	
Value of r_2 for n = 2.14 (Figure 7) Dimensionless	= 0.587
On tracing = 0.587/1.715 × 47	= 16.1 units
Value of h from tracing = 64 − 16.1	= 47.9 units
Value of j	= 14.5 units
Angle $\theta_1 = \tan^{-1}$ 14.5/47.9	= 16.9°

Using values for n and θ_1 of 2.1 and 17° respectively, the area and volume were found from Tables 2 and 3,

Area	= 11.37 square units	
	= 11.37 × $(0.201)^2$	= 0.459 cm.^{2}
Volume	= 3.744 cubic units	
	= 3.744 $(0.201)^3$	= 0.0304 cm.^{3}

As the bubble began to break away, an elongated neck was formed which rapidly collapsed until rupture. To calculate areas and volumes for these shapes, the neck was assumed to be made up of frusta of right cones.

For the system Paraffinol-n-hexane-nitrogen the odd shapes at the beginning of formation were assumed to be oblate spheroids or composed of one-half of a sphere and one-half of an oblate spheroid.

(c) Variation of Bubble Area During Formation

From each length of film for the five different diameters, bubble shapes were traced and the area and volume calculated.

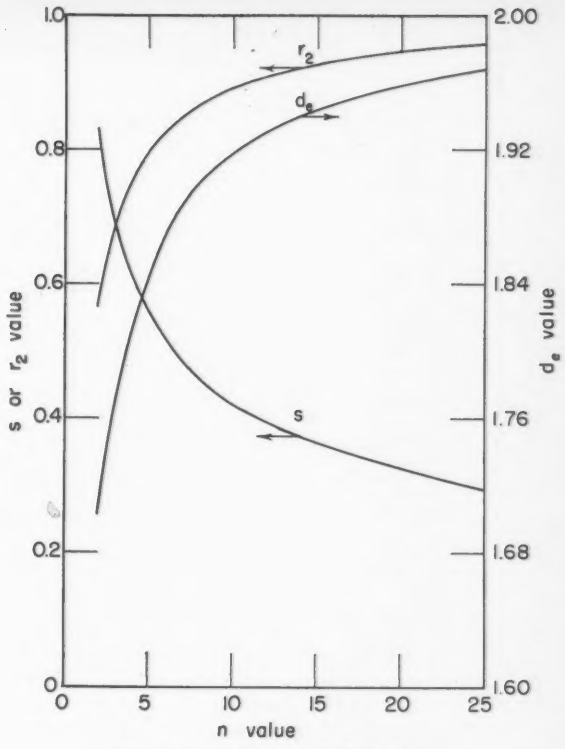

Figure 7—Values for bubble shape.

For the system Paraffinol-n-hexane-nitrogen, Figures 8 and 9 show the volume and area variation respectively. The time scale was plotted as $t_f - t$, with t_f as the formation time and t as the time starting at bubble growth. Since the frequency varied slightly this method of plotting was preferred.

None of the curves were linear so approximate variations with time were sought as this was important for the mass transfer study. The volume varied as time to a fractional power as indicated by the equations and curves drawn on Figure 9, the particular exponents are empirical. Then, assuming the bubble to be spherical during growth, meant that the area should vary with time as two-thirds of the power used for the volume. This proved correct in Figure 9.

However, to show that the previous conclusion would not hold in every case, plots of volume and area variation for a nitrogen bubble in water were shown in Figures 10 and 11. The volume growth was quite linear with time which would have suggested that area varied as two-thirds power of time. This was not so as the area varied quite linearly for most of the formation time.

It was for this reason that bubble growth was investigated so thoroughly. For the mass transfer work a definite difference in the amount of transfer during formation was predicted depending on the area variation.

(d) Formation Time

From all of the film taken of bubbles forming at a nozzle, the formation time, t_f, was recorded. In Figure 12 this time was plotted against the flow rate. At first it was assumed that the formation time would vary with frequency but a check at frequencies of 151 and 420 proved otherwise. The flow rate was the most important variable.

The points for Figure 12 were obtained on three separate days and there was a vertical deviation as shown. Even though extreme care was taken in cleaning the apparatus, especially the nozzle, some contamination must have made the results deviate.

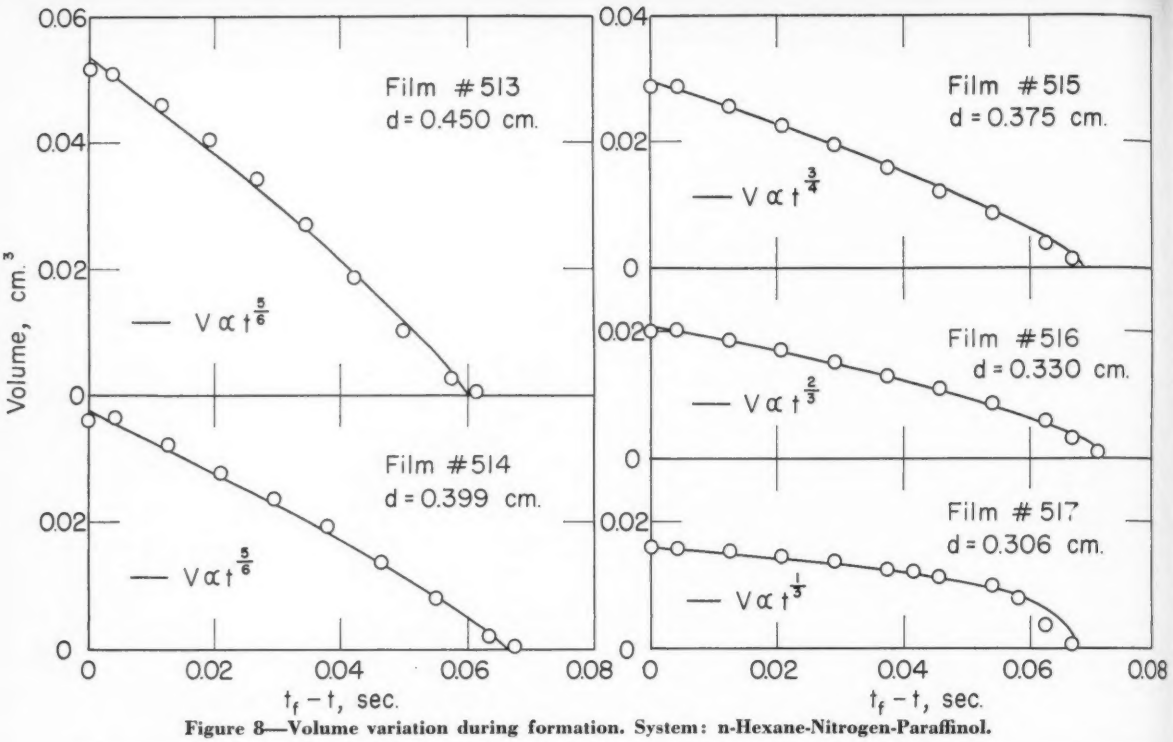

Figure 8—Volume variation during formation. System: n-Hexane-Nitrogen-Paraffinol.

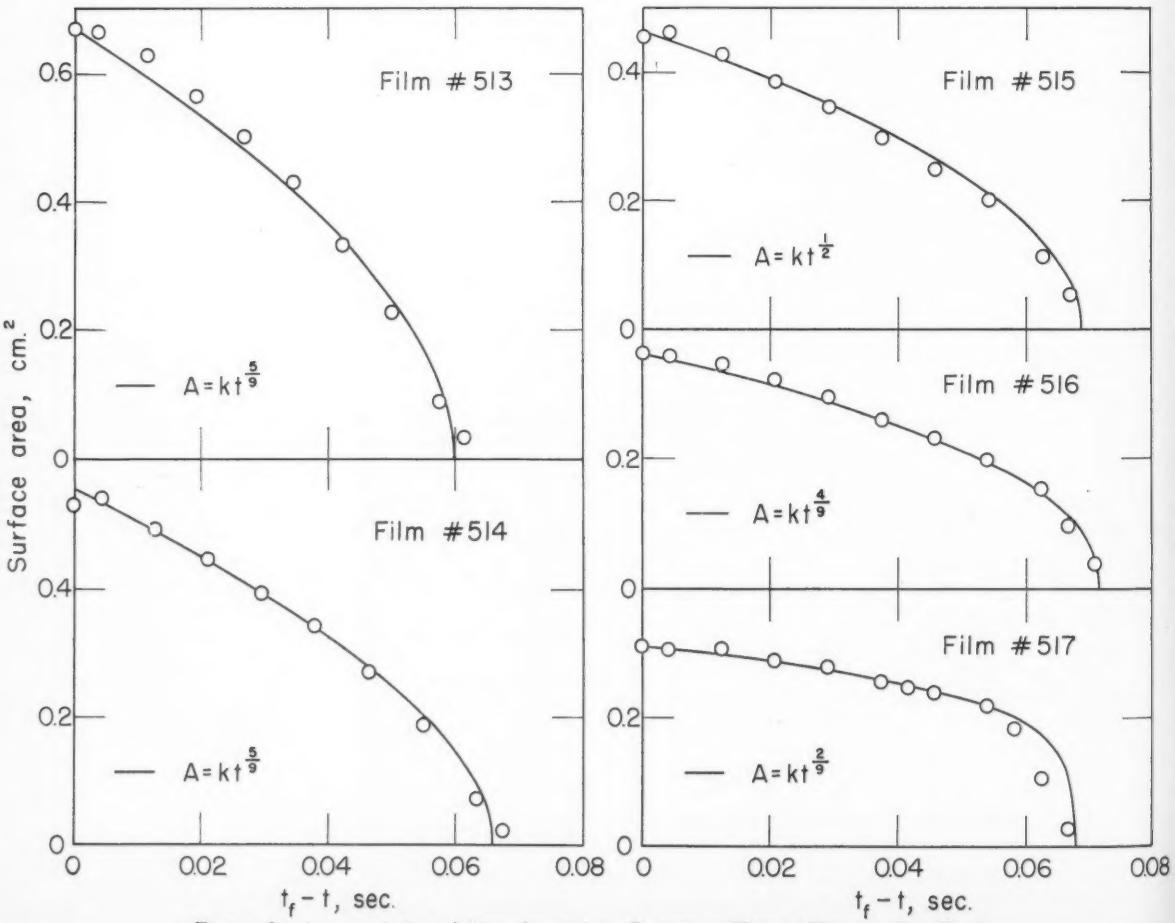

Figure 9—Area variation during formation. System: n-Hexane-Nitrogen-Paraffinol.

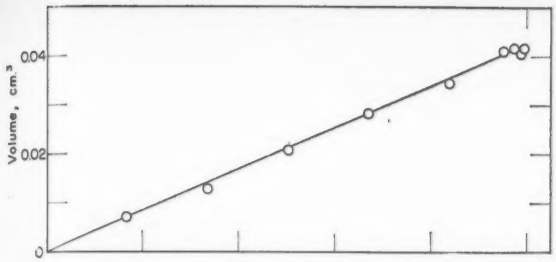

Figure 10—Volume variation during formation. System: Nitrogen-Water.

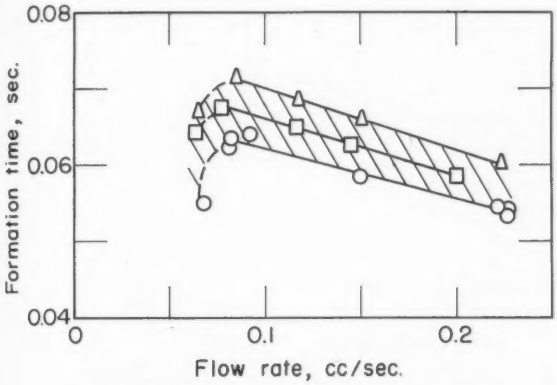

Figure 12—Formation time versus flow rate.

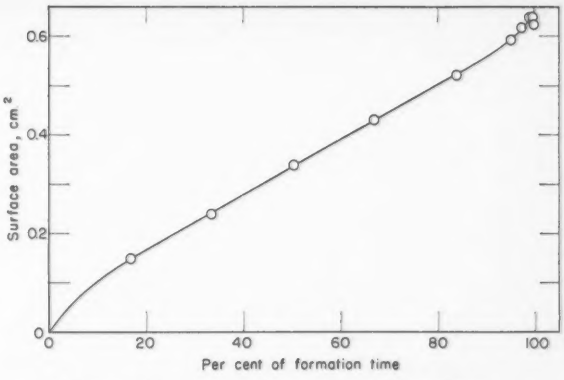

Figure 11—Area variation during formation.

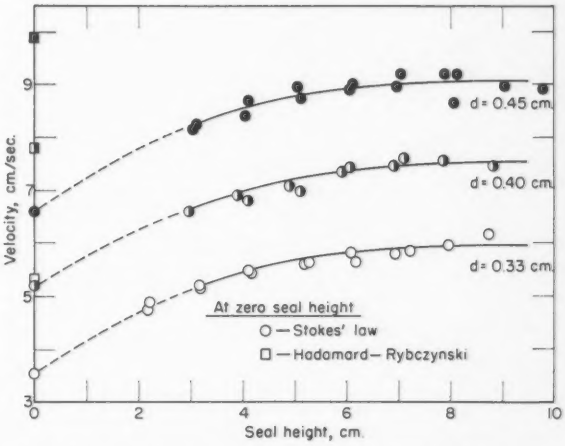

Figure 13—Bubble velocities. System: Paraffinol-n-Hexane-Nitrogen.

However, on any particular day the formation time decreased with increasing flow rate. At the lowest flow rate, i.e. smallest bubble size, the valve on the inlet line for controlling the frequency, had to be closed almost completely. This gave a smaller formation time, deviating from a linear plot through the other points.

(e) Bubble Rise Velocity

(1) *Heavy oil — Paraffinol* For the system Paraffinol-n-hexane-nitrogen, typical curves of bubble velocities at different seal heights and bubble diameters were plotted in Figure 13. As the seal height was increased, the velocity increased, which suggested that the continuous phase was moving upward in the bubble path and was helping the motion of the bubbles with respect to the column. At higher seal heights, when the circulation in the column became more developed, the bubble velocity remained constant. Actual observation of small trapped bubbles in the continuous phase confirmed the circulation of the oil.

The velocity curves in Figure 13 were quite similar and it was interesting to find what the velocity would be at zero seal height when theoretically the oil phase had no effect on the bubbles. Several workers[11,12] studied the rise of single air bubbles in hydrocarbon oils similar to that in this work, and they found that the bubbles did circulate inside. They assumed this circulation since the velocity was that predicted by the Hadamard-Rybczynski theory. This would seem to suggest that the intercepts in Figure 13 should be those calculated from Equation[12]. However, it was discovered that the intercepts could be better represented by Stokes' law as shown by the dashed lines in Figure 13. From this a very useful but limited correlation was proposed for this study.

A general curve of the difference between actual and Stokes' law velocity was plotted against seal height. A later modification changed the seal height to the height of rise, i.e. the true distance the bubble rose. This height of rise was calculated by subtracting from the seal height the distance from the top of the bubble to the nozzle tip immediately after release. Figure 14 was prepared from the movie film of bubble formation and it gave the maximum height of the bubble above the nozzle mouth after release.

Figure 15 shows the velocity difference from Stokes' law versus the height of rise. The majority of this data was at a frequency approximately 270 per minute to correspond with later mass transfer work. Several points were recorded at low seal heights for the other frequencies needed. Some of the mass transfer work was at a frequency of 192 per minute and the velocity data were estimated from a cross-plot of velocity difference versus frequency with height of rise as the parameter.

The best curve through the data at $f = 270$ per minute was calculated by least squares analysis assuming a polynomial distribution. The solution was easily obtained from a prepared program for the I.B.M. 650 computer in the Physics Department.

The curve in Figure 15 did not pass through the origin since acceleration of the bubble took place at low seal heights.

It was assumed that circulation still existed in the bubbles and any agreement with Stokes' law rather than the Hadamard-Rybczynski modification was superficial. The range of Reynolds numbers for the heavy oil was from 0.6 to 1.8 which was just at the transition of the curve of the drag coefficient versus Reynolds number. The drag curve began to deviate from Stokes' law at this point. Also, Garner and Hammerton[12] found that bubbles behaving like fluid spheres with a velocity predicted by Hadamard-Rybczynski, had their velocities decreasing towards the solid sphere velocity curve in the Reynolds number region from 0.1 to 10. Since the author's work was in this region the correlation was probably fortuitous.

(2) *Light oil* For the system light oil-n-hexane-nitrogen velocity data for a bubble diameter of 0.34 cm. were plotted in Figure 16. This curve was essentially the same as that in

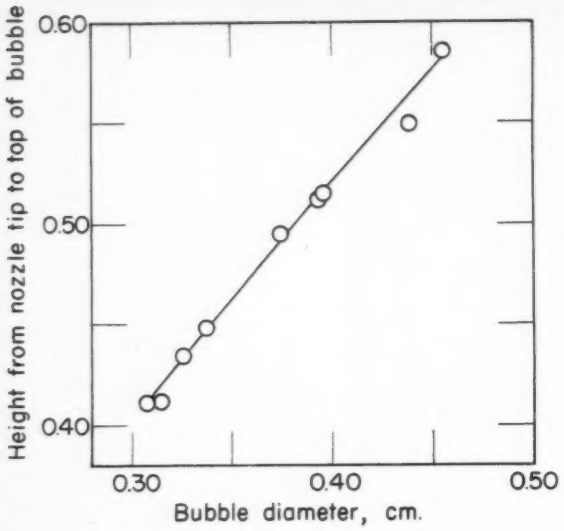

Figure 14—Height of bubble just before release.

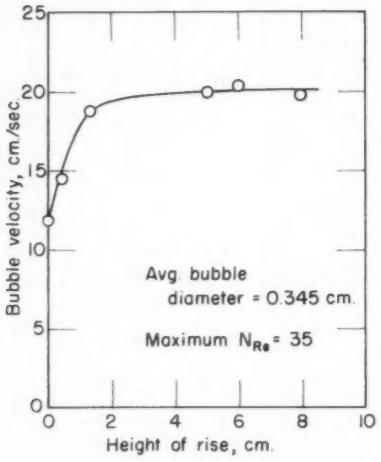

Figure 16—Bubble velocity. Light oil.

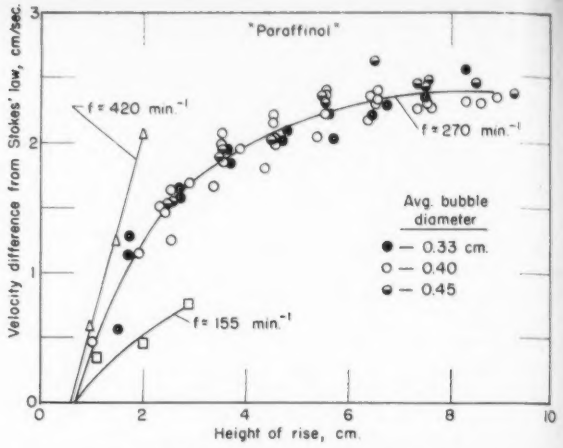

Figure 15—Bubble velocities at different frequencies.

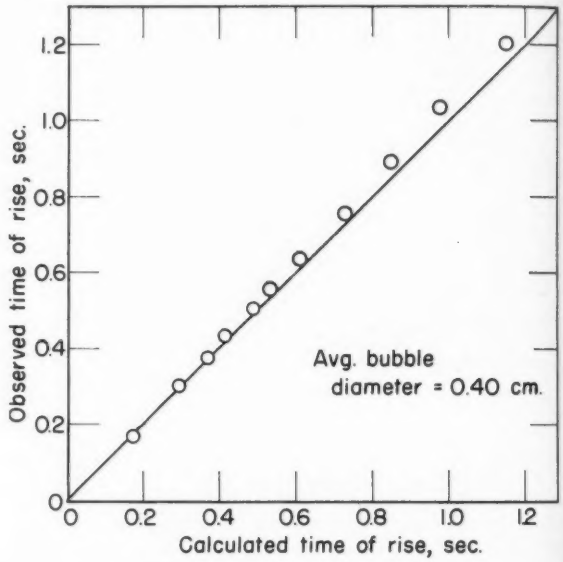

Figure 17—Observed versus calculated time of rise.

Figure 13. However, the velocity at zero seal height was calculated from a plot of drag coefficient versus Reynolds number (Perry's Handbook[25]).

(3) *Wall effect* Uno and Kintner[26] studied the rise of air bubbles through several liquids and found very little wall effect if the ratio of column diameter to bubble diameter was ten or greater. Although the Reynolds number range of their work was greater (above 20) than in this study, since with the largest bubble diameter used in this work the ratio was greater than 15, it was assumed that no wall effect was present with either column used, that is the 3″ round and the 4″ square column.

(f) Time of Rise

For later mass transfer work the contact time for the rise period was needed. This was calculated by dividing the height of rise by the actual velocity of the bubble. From the bubble diameter, Stokes' law velocity, and Figure 15, the contact time of the bubble for a certain seal height could be estimated.

From movie film for a bubble diameter of 0.40 cm. the actual observed contact time was recorded and plotted with the calculated time of rise. Figure 17 shows the greatest deviation at high contact times. This deviation became much less at the lower times at which the important mass transfer work was done.

Conclusions

Bubble shapes during formation were predicted quite well by $r_n\theta = 1$ with n as a variable power. This equation may not be as accurate for static bubbles as the theoretical one derived by Bashforth and Adams but it had a less complex form.

In many instances bubble volume growth during formation had been assumed spherical and linear with time. The surface area computed from a spherical bubble would then vary as the two-thirds power of time. This assumption would not be correct in every case since surface tension, dynamic forces, and nozzle size could combine to give very different results. Each study of bubble formation, especially in mass transfer work, should include the determination of area variation since the amount of mass transferred will be affected.

A limited correlation was found for the velocity of rise of a chain of bubbles in a heavy mineral oil. The actual velocity was greater than Stokes' law velocity and varied with seal height. The difference between the two at each seal height was constant in the range of bubble diameters studied, i.e. 0.33 to 0.45 cm. It was difficult to determine if any circulation existed inside of the bubbles but based on the work in other references[11,12] on similar systems, circulation seemed very likely. The agreement with Stokes' law was therefore fortuitous.

Nomenclature

A = bubble surface area, cm.^{2}
b = radius of curvature for theoretical bubble shape
d = bubble diameter, cm.
d_s = bubble width during formation
e, h, j = measurement of bubble shape.
f = bubble frequency, min.$^{-1}$
g = acceleration constant, cm./sec.^{2}
k = constant in $A = kt^y$
$k = \dfrac{2\mu + 3\mu_i}{3\mu + 3\mu_i}$
n = variable power in $r^n\theta = 1$
N_{Re} = Reynolds number.
r = bubble radius, cm.
r = polar coordinate.
t_f = formation time, sec.
v = bubble velocity, cm./sec.
V = bubble volume, cc.
y = exponent in $A = kt^y$

Greek

β = shape factor.
θ_1 = angle between polar axis and nozzle edge.
μ = liquid viscosity, centipoises.
μ_i = viscosity inside sphere, centipoises.
γ = kinematic viscosity, cm.^{2}/sec.
ρ_G = gas density, gm./cc.
ρ_L = liquid density, gm./cc.
ρ = radius of curvature for theoretical shape.
$\dfrac{x}{\sin\phi}$ = radius of curvature for theoretical shape.
σ = surface tension, dynes/cm.

References

(1) Bashforth, F., and Adams, H., Capillary Action, Cambridge (1883).
(2) Worthington, A. M., Phil. Mag. **19,** 46 (1885).
(3) Ferguson, A., Phil. Mag. **23,** 417 (1912).
(4) Andreas, J. M., Hauser, E. A., and Tucker, W. B., J. Phys. Chem. **42,** 1001 (1938).
(5) Fordham, S., Proc. Roy. Soc. **A194,** 1 (1948).
(6) Siemes, W., Chem. Ing. Tech. **26,** 479 (1954).
(7) Lane, W. R., and Green, H. L., "The Mechanics of Drops and Bubbles", Survey in Mechanics, Edited by G. K. Batchelor and R. M. Davies, Cambridge U. Press.
(8) Wark, I. W., J. Phys. Chem. **37,** 623 (1932).
(9) Freud B. B., and Harkins, W. D., J. Phys. Chem. **33,** 1217 (1929).
(10) Null, H. R., and Johnson, H. F., A.I.Ch.E. Journal **4,** 273 (1958).
(11) Haberman, W. L., and Morton, R. K., Pro. Amer. Soc. Civil Engrs. **80,** No. 387 (1954).
(12) Garner, F. H., and Hammerton, D., Chem. Eng. Sci. **3,** 1 (1954).
(13) Peebles, F. N., and Garber, H. J., Chem. Eng. Prog. **49,** 88 (1953).
(14) O'brien, M. P., and Gosline, J. E., Ind. Eng. Chem. **27,** 1436 (1935).
(15) Robinson, J. V., J. Phys. and Colloid Chem. **51,** 431 (1947).
(16) Datta, R. L., Napier, D. G., and Newitt, D. M., Trans. Inst. Chem. Engrs. **28,** 14 (1950).
(17) Stokes, G. G., Mathematical and Physical Papers, Vol. 1, Cambridge U. Press (1880).
(18) Hadamard, J., Compt. Rend. **152,** 1735 (1911).
(19) Rybczynski, Bull. Acad. Sci. Cracovie **1,** 40 (1911).
(20) Bond, N. W., and Newton, D. A., Phil. Mag. **5,** 794 (1928).
(21) Coppock, P. D., and Meiklejohn, G. T., Trans. Inst. Chem. Engrs. **29,** 75 (1951).
(22) Guyer, A., and Pfister, X., Helv. Chim. Acta. **29,** 1173 (1946).
(23) Owens, J. S., Engineering **112,** 458 (1921).
(24) Lamb, H., Hydrodynamics, Cambridge U. Press 6th Ed. (1952).
(25) Perry, J. H., Chemical Engineers' Handbook McGraw-Hill 3rd Ed. (1950).
(26) Uno, S., and Kintner, R. C., A.I.Ch.E. Journal **2,** 420 (1956).

★ ★ ★

Kinetics of the Vapor-Phase Oxidation of Napthalene over a Vanadium Catalyst[1]

K. A. SHELSTAD[2], *J. DOWNIE*[3], *and W. F. GRAYDON*[4]

Rates of oxidation of naphthalene were measured for the temperature range 300°C. to 335°C. using a thin layer of vanadium oxide-potassium sulfate-silica catalyst in a flow reactor. The amounts of naphthalene converted were determined by analysing the products for 1,4-naphthoquinone, 1,2-naphthoquinone, and phthalic anhydride. Negligible amounts of products of complete combustion were formed.

The reaction rate data obtained at low conversions of naphthalene were correlated by the following expression, based upon a model for the reaction proposed by Hinshelwood:

$$r_n = \frac{k_a\, k_n\, C_n\, C_o}{k_a\, C_o + N\, k_n\, C_n}$$

From the results of experiments in which the contact time was varied, it was suggested that the reaction course consisted of two parallel, consecutive reactions in which 1,4- and 1,2-naphthoquinone are intermediates in the formation of phthalic anhydride.

During the past 40 years numerous experiments have been carried out on the oxidation of naphthalene in the vapor-phase over a contact catalyst. A large number of these experiments were concerned with the catalytic properties of various preparations and the determination of conditions for producing phthalic anhydride.

The earliest of these studies indicated that the main products of the reaction were naphthoquinone, phthalic anyhdride, maleic anhydride, carbon dioxide and water. Since these can be arranged in a series representing an increase in the degree of oxidation of the parent compound naphthalene, it was usually supposed that these products were formed through a series of consecutive reactions. Direct evidence in support of this view was lacking, however, since in these early experiments conversions were large and temperature control of the reacting mass inadequate.

Beginning with the experiments reported by Calderbank[1] in 1952, several investigators have contributed towards an understanding of the kinetics of this reaction. Although there is considerable agreement that the reaction is first-order with respect to the concentration of oxygen, the order with respect to the naphthalene concentration is zero according to Calderbank[1], first according to D'Alessandro and Farkas[2], while Ioffe and Sherman[3] assumed this order to be zero and that inhibition by the reaction products was taking place. Mars and van Krevelen[4], on the other hand, treated the reaction in terms of two processes, the first being first-order in the naphthalene concentration and the second first-order in the oxygen concentration, with a varying steady-state concentration of oxygen on the catalyst surface. Since the conditions used in these studies varied considerably, it is possible that these differences of opinion concerning the reaction order with respect to the naphthalene concentration are more apparent than real.

Apparatus

Figure 1 is a flow diagram of the apparatus used for the oxidation experiments. A mixture containing known amounts of oxygen, nitrogen, and naphthalene entered at the bottom of the reactor. These gases passed through the thin bed of catalyst and then left the reactor through a glass head and passed to an air condenser and a cold trap. Filters of cotton were placed between the air condenser and the trap, and near the exit from the trap. A drop or two of paraffin oil of low volatility was usually placed on the last filter.

The carburetors were made from 25 mm. Pyrex tubing with a porous glass disk near the bottom.

A diagram of the reactor is shown in Figure 2. This was constructed from a 20-inch length of 1-inch, schedule 40, stainless steel pipe located centrally within a 12-inch length of 6-inch steel pipe, and the annular space filled with aluminum. The upper end of the central pipe was machined to take a 29/42 standard glass taper used to make connection with the glass reactor head. An ordinary pipe flange at the lower end of the reactor tube served to join this with a short piece of Pyrex pipe and its flange. The gasket between the two flanges was of Teflon. The outside of the 6-inch pipe was covered by a layer of mica, over which was placed the electrical resistance windings of Chromel ribbon. These were then covered by a thin layer of Zauer-reisen cement, followed by a 2-inch layer of magnesia blocks.

A piece of 100-mesh, stainless steel screen was pressed into the central pipe to serve as support for the catalyst.

The temperature was measured at two points by calibrated Chromel-Alumel thermocouples. The thermocouple inside the central tube of the reactor was protected by a sheath made from 18 mm. Pyrex tubing. This left a narrow annulus between the sheath and reactor walls to aid in removing quickly the product gases from the system. During an oxidation run the lower end of the sheath was about ⅛ of an inch above the catalyst bed. The temperature indicated by this thermocouple

[1]*Manuscript received January 22; accepted April 20, 1960.*
[2]*Assistant Professor, Department of Chemical Engineering, McGill University, Montreal, Que.*
[3]*Gulf Research and Development Company, Pittsburgh, Pa.*
[4]*Professor of Chemical Engineering, Department of Chemical Engineering and Applied Science, University of Toronto, Toronto, Ont.*
Contribution from the Department of Chemical Engineering and Applied Science, University of Toronto, Toronto, Ont. Based on a paper presented to the C.I.C. Chemical Engineering Conference, November 9-11, 1959.

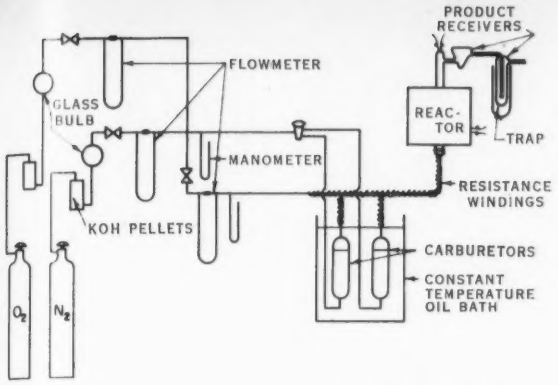

Figure 1—Flow diagram of apparatus for catalytic oxidation of naphthalene.

was recorded as the temperature of the catalyst bed. The second thermocouple was located near the outside surface of the central pipe by means of a hole drilled through the aluminum block. A Bristol model 560 Dynamaster was used to record the temperature indicated by each thermocouple and to regulate the power input to the electrical resistance windings on the outside of the reactor. The sensitive element in this control was the thermocouple in the aluminum block. For most of the oxidation runs the two thermocouples gave the same temperature reading; at times, however, the temperature in the aluminum block was about 1 C. degree higher.

Operating Procedure

The operating procedure involved, in the first place, a preliminary oxidation run of 1-2 hours. The purpose of this was to permit the system, particularly the catalyst, to attain a steady-state condition. A run proper was then started by replacing an auxiliary condenser by a weighed air condenser and switching the primary gas stream from the unweighed naphthalene carburettor. The time for these runs varied from three-quarters of an hour to two hours. At the end of a day's operation nitrogen was passed through the reactor for at least 30 minutes before the current to the electrical heaters was turned off.

Materials Employed

Naphthalene was B.D.H. Certified chemical. Melting point 80.0°C.

Benzene was Fisher Certified Chemical, thiophene-free.

Oxygen and nitrogen were taken from cylinders containing the compressed gases. They were dried over solid potassium hydroxide before being passed to the reactor.

1,4-Naphthoquinone (Fisher) was recrystallized from ether as suggested by Fieser[5] (melting point 125°C. corrected).

1,2-Naphthoquinone was prepared from Orange-2 using the procedure outlined by Fieser[5]. The material did not give a sharp melting point but softened and turned black at about 140°C. It consisted of tiny needles colored a golden orange.

The catalyst was obtained from Imperial Smelting Corporation Limited, Avonmouth, England. It was taken from a large batch of catalyst of which the mean analysis was:

V_2O_5 = 9.95 % K_2O = 14.7 %
Fe = 0.16 % SO_3 = 18.6 %
Loss on ignition = 12.5 %
The remainder mainly silica.

All analyses are expressed as a percentage of the catalyst ignited to 800°C., except the SO_3 figure which is expressed on the sample dried at 110°C.

All the naphthalene conversion rates reported in this paper were carried out using a single sample of this catalyst weighing

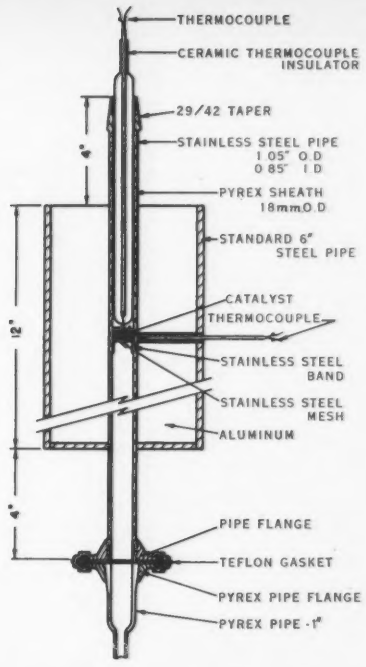

Figure 2—Reactor for catalytic oxidation of naphthalene.

1.130 grams. The size of the particles in this sample was kept uniform by spreading out the crushed catalyst on graph paper and picking out by hand only those pieces which fitted a square 0.05 inches on a side.

Identification of Reaction Products and Methods of Analysis

Phthalic anhydride was qualitatively identified in the reaction products by fusion with resorcinol and formation of the dye fluorescein[6]. It was determined quantitatively by titration with 0.02 *N NaOH* using phenolphthalein as indicator. A direct titration was found to be unsatisfactory due to the end-point being obscured by the small solubility of naphthoquinone in the aqueous solution. Therefore, the product solution in benzene was first extracted with 0.02 *N NaOH*, the aqueous layer acidified with 0.02 *N HCl*, this solution extracted once with benzene to remove naphthoquinone, the aqueous layer boiled to remove carbon dioxide, and final adjustment to the end-point made after cooling the solution to room temperature.

1,4-Naphthoquinone was identified in the reaction products by measuring the absorption spectrum of a benzene solution of the products after this solution had been extracted several times with 0.02 *N NaOH*. A Beckman *DU* quartz spectrophotometer was used to make the measurements. The position of the peaks in the region 325 mμ to 600 mμ, as well as the relative extinction coefficients of these peaks, agreed closely with the measurements reported by Nagakura and Kuboyama[7] and as determined with a sample of pure 1,4-naphthoquinone in benzene.

During the period when preliminary runs were being carried out it was noticed that the products contained an orange-colored substance. The only colored substance expected from information in the literature was 1,4-naphthoquinone, which is colored a bright, canary yellow. It was also noticed that if the products stood open to the atmosphere, a color change to dark green occurred in 2-3 days time. A number of experiments were then made in an attempt to discover the nature of this unknown substance. In one instance, the total naphthoquinone content was determined by ceric sulfate titration (method outlined below) and by a Klett-Summerson colorimeter calibrated for 1,4-naphthoquinone. The value determined colorimetrically was

several times larger than that found by titration. This indicated that a substance was present which has an extinction coefficient greater than that of 1,4-naphthoquinone at the wavelengths used in the colorimeter (band maximum 420 mμ). It was postulated that the unknown substance was 1,2-naphthoquinone. As a test of this, the products from 20 runs were analysed for total naphthoquinone by titration with ceric sulphate solution and by extinction measurements using extinction coefficients determined from pure samples of 1,4- and 1,2-naphthoquinone. In 18 of these runs the two methods gave the same naphthoquinone content within experimental error. In another series of tests synthetic mixtures were prepared containing, in one case, naphthalene, phthalic anhydride, and 1,4-naphthoquinone, and in a second case, 1,2-naphthoquinone as well as the other constituents. These mixtures were let stand open in the laboratory. Only the mixture containing 1,2-naphthoquinone developed a green color after 2-3 days.

The chemical method used to analyse for naphthoquinone was that previously outlined by Rosin et al[8]. 25 ml. of a benzene solution of the reaction products was treated with 10 ml. of glacial acetic acid and 0.5 gm. of zinc dust. When the solution was colorless, the mixture was diluted with water, filtered, and titrated with standard ceric sulfate solution using o-phenanthroline as indicator.

For the extinction measurements a Beckman *DU* quartz spectrophotometer with matched cells of silica was employed. Solutions of 1,4- and 1,2-naphthoquinone, respectively, were shown to follow Beer's law at wavelengths 340 and 540 mμ.

The product gases from 23 runs in the temperature range 312° to 352°C. were analyzed for carbon dioxide by determining the increase in weight of an absorber containing Carboxite. In all but two of these runs the amounts of carbon dioxide were found to be equivalent, within experimental error, to the amounts of anhydride formed. It was therefore concluded that products corresponding to oxidation beyond the phthalic anhydride stage were not formed under the conditions of temperature and contact time employed.

The moles of 1,4- and 1,2-naphthoquinone and phthalic anhydride in the product gave, therefore, the moles of naphthalene oxidized during the run. This value, together with the number of grams of catalyst in the reactor and the length of the run in seconds, was used to calculate the naphthalene conversion rate in moles of naphthalene oxidized per gram of catalyst per second.

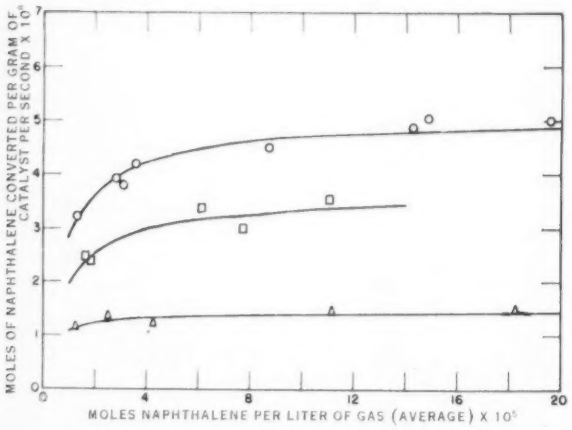

Figure 3—Rate of oxidation of naphthalene as a function of the average concentration of naphthalene in the bed of catalyst. Temperature 312°C. Oxygen concentration: △, 2.08 x 10^{-3} moles per liter; □, 4.64 x 10^{-3} moles per liter; ○, 6.86 x 10^{-3} moles per liter.

Experiments with No Catalyst in the Reactor

A number of runs were carried out under conditions similar to those during the catalytic runs but with no catalyst in the reactor. The products obtained contained no acidic substances but were colored faintly yellow. Extinction measurements were carried out at 340 mμ on solutions of these products in benzene and the results interpreted in terms of 1,4-naphthoquinone content. Comparison of these amounts of 1,4-naphthoquinone with those formed during the catalytic experiments indicated that the non-catalyst formation of naphthoquinone is one percent or less of that formed during the catalytic runs. No correction to the measured catalytic rates was therefore made.

Oxidation Runs at Low Naphthalene Conversions

In this series of runs the results were plotted as naphthalene conversion rate versus the arithmetic average of the naphthalene concentration entering and leaving the catalyst bed, with oxygen concentration as a parameter. In Figure 3 the results are shown for a temperature of 312°C.; in Figure 4, for a temperature of 335°C. These curves show that the conversion rate is dependent upon the naphthalene concentration at low values of the naphthalene concentration and high values of the oxygen concentration. At high concentrations of naphthalene, however, the conversion rate is nearly independent of the concentration of naphthalene.

Although oxidation of the naphthalene most probably occurs on or near the catalyst surface, it is possible that the rate of adsorption of one reactant is of the same order of magnitude as the rate of the chemical reaction. In the following treatment, the method outlined by Hinshelwood[9] is used. If it is supposed that oxygen only is adsorbed on the catalyst surface, that the rate of desorption of oxygen is negligible, and that reaction occurs when naphthalene in the gas phase strikes adsorbed oxygen, then it can be expected that a steady-state will be established wherein the rate of removal of oxygen by chemical reaction is equal to the rate of adsorption of oxygen. Thus:

$$k_a C_o (1 - S) = k_o C_n S \quad \ldots\ldots\ldots\ldots\ldots\ldots (1)$$

If N is the number of moles of oxygen consumed for each mole of naphthalene reacting, then:

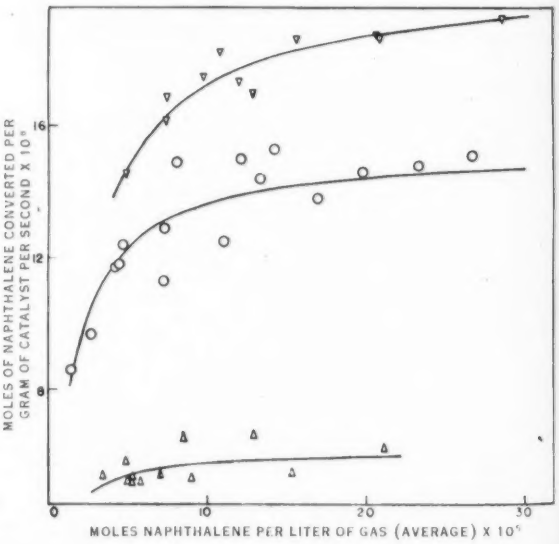

Figure 4—Rate of oxidation of naphthalene as a function of the average concentration of naphthalene in the bed of catalyst. Temperature 335°C. Oxygen concentration: △, 3.00 x 10^{-3} moles per liter. ○, 6.61 x 10^{-3} moles per liter; ▽, 8.81 x 10^{-3} moles per liter.

$$\text{rate of naphthalene oxidation} = k_n C_n S \quad \ldots\ldots\ldots\ldots (2)$$
$$= (1/N)\ (\text{rate of reaction of oxygen})$$

From (1) and (2), the rate of oxidation of naphthalene is written:

$$r_n = \frac{k_a k_n C_n C_o}{k_a C_o + N k_n C_n} \quad \ldots\ldots\ldots\ldots\ldots\ldots (3)$$

For constant oxygen concentration, Equation (3) becomes:

$$r_n = \frac{k_n C_n}{1 + K_1 C_n} \quad \ldots\ldots\ldots\ldots\ldots\ldots (4)$$

When inverted, the equation is easy to use for purposes of correlating the data.

$$\frac{1}{r_n} = \frac{1}{k_n}\frac{1}{C_n} + K_2 \quad \ldots\ldots\ldots\ldots\ldots\ldots (5)$$

Using Equation (5) and the method of least squares, the most probable value for constants $1/k_n$ and K_2, respectively, was calculated from the experimental data. Using these values in Equation (4) the r_n vs. C_n curve was calculated. These curves are given by the full lines in Figures 3 and 4. It can be seen that a reasonable fit of the data is obtained at constant oxygen concentration. Values for the constants of Equation (4) are given in Table 1. In this table, N is the average of the individual values for each series of runs at constant oxygen concentration.

Additional values of k_a were obtained from runs at high concentrations of naphthalene where the reaction rate is essentially independent of the naphthalene concentration. For such conditions, Equation (3) predicts:

$$r_n = \frac{k_a C_o}{N} \quad \ldots\ldots\ldots\ldots\ldots\ldots (6)$$

Since the values of r_n, C_o, and N are all measured, k_a is readily calculated. Particulars concerning these runs are listed in Table 2.

The specific velocity constants, k_n and k_a, are expected to be constant at a given temperature. In the case of k_a this is approximately so. However, considerable variation was found for k_n. This variation does not appear to be due to a change in the concentration of oxygen.

The oxygen dependence of the rate was checked at 335°C. by plotting naphthalene conversion rate versus oxygen concentration for a series of runs in which the naphthalene concentration was greater than 12×10^{-5} moles per liter. In this range the rate of oxidation of naphthalene is nearly independent of the concentration of naphthalene. The curve obtained (see Figure 5) is essentially linear, extrapolating through the origin. It is concluded, therefore, that the naphthalene conversion rate is first-order in the oxygen concentration.

Since the shape of the curves in Figures 3 and 4 is similar to Langmuir-type adsorption isotherms, it may be argued that a method of correlating the data may be possible based on a surface reaction between adsorbed reactants. This was indeed tried, and, although a slightly better correlation of the data was obtained, interpretation of the constants of the resulting equation proved to be difficult. The expression obtained was more complicated than (3). It is for this reason, together with the fact that there is considerable scatter in the data available at the present time, that the simpler Hinshelwood approach is preferred.

Naphthalene Conversion at Longer Contact Times

In an additional series of runs at 335°C. the concentration of oxygen and of naphthalene was kept approximately constant while the contact time was varied by changing the gas flow rate. The results obtained are presented graphically in Figure 6. In the figure the reciprocal of the gas flow rate is plotted on the abscissae since this is directly proportional to the contact time for a fixed amount of catalyst. It is seen that the concentration of 1,4-naphthoquinone and phthalic anhydride increase almost linearly over the range of flow rates used, while, over this same range, a decrease in the concentration of 1,2-naphthoquinone occurs.

To interpret these results in terms of the reaction course, it is supposed, first of all, that 1,4- and 1,2-naphthoquinone are formed through two separate reactions occurring simultaneously. This is reasonable since it is doubtful that either quinone can be formed from the other under the conditions of the oxidation experiments. In the second place, a reaction leading to the removal of 1,2-naphthoquinone is involved since the concentration of this quinone decreases for an increase in the contact time (see Figure 6). Concerning the formation of phthalic anhydride three possible sources are considered:

(1) Phthalic anhydride is formed by a process parallel to the formation of 1,4- and 1,2-naphthoquinone.
(2) Phthalic anhydride is formed from 1,4-naphthoquinone.
(3) Phthalic anhydride is formed from 1,2-naphthoquinone.

With regard to point (1) that a third simultaneous reaction gives rise to the phthalic anhydride, a plot of the moles of anhydride per mole of 1,4-naphthoquinone in the product versus the reciprocal of the gas flow rate should be horizontal, unless the two reactions are of different order with respect to the naphthalene concentration. Such a plot is given in Figure 7, from which it is seen that this ratio increases with the contact time. Therefore, either phthalic anhydride is not formed solely through a third simultaneous reaction, or else the two reactions are of different order with respect to the naphthalene concentration. It is the author's opinion that such a difference of order is unlikely. Concerning point (2) that 1,4-naphthoquinone is an intermediate in the formation of phthalic anhydride, the slope of the curve in Figure 6 should decrease as the contact time is increased. Clearly, no significant effect of this kind is indicated. That 1,2-naphthoquinone is an intermediate in the formation of phthalic anhydride, as suggested in point (3), is quite possible, however. Figure 6 shows that the concentration of this quinone decreases with contact time as expected for an intermediate in two consecutive reactions. It is therefore concluded that the data represented in Figures 6 and 7 are consistent with a reaction scheme involving two parallel, consecutive reactions:

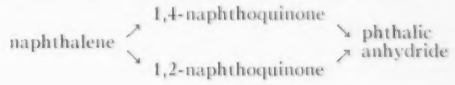

TABLE 1

CONSTANTS OF EQUATIONS (3) AND (5)

T °C.	C_o x 10^3	$1/k_n$	$K_2 = K_1/k_n$ x 10^{-5}	k_n x 10^3	k_a x 10^5	N
312	6.86	161	197	6.21	1.80	2.43
312	4.64	242	274	4.14	1.94	2.47
312	2.08	245	681	4.09	1.57	2.23
335	8.81	94.5	48.77	10.6	5.91	2.54
335	6.61	81.1	65.35	12.3	6.00	2.59
335	3.00	122	161.2	8.20	5.19	2.51

TABLE 2

REACTION RATES AT HIGH CONCENTRATIONS OF NAPHTHALENE

T °C.	r_n x 10^5	C_o x 10^3	N	k_a x 10^5
300	1.53	3.16	2.68	1.30
300	1.48	3.12	2.72	1.29
312	2.36	3.07	2.58	1.98
312	2.32	3.08	2.60	1.96
324	3.88	3.01	2.72	3.50
324	3.95	2.99	2.70	3.57

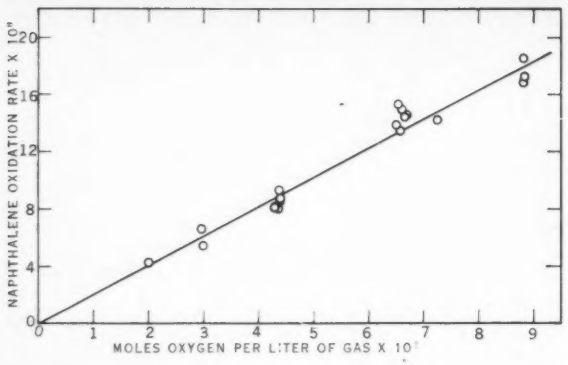

Figure 5—Rate of oxidation of naphthalene as a function of oxygen concentration for concentrations of naphthalene greater than 12 x 10^{-5} moles per liter. Temperature 335°C.

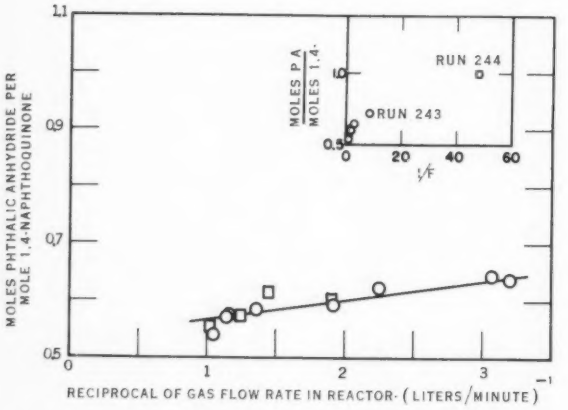

Figure 7—Relative amounts of phthalic anhydride and 1,4-naphthoquinone formed in the catalyst bed after different contact times. Oxygen concentration: ○, 6.6 x 10^{-3} moles per liter; □, 4.4 x 10^{-3} moles per liter.

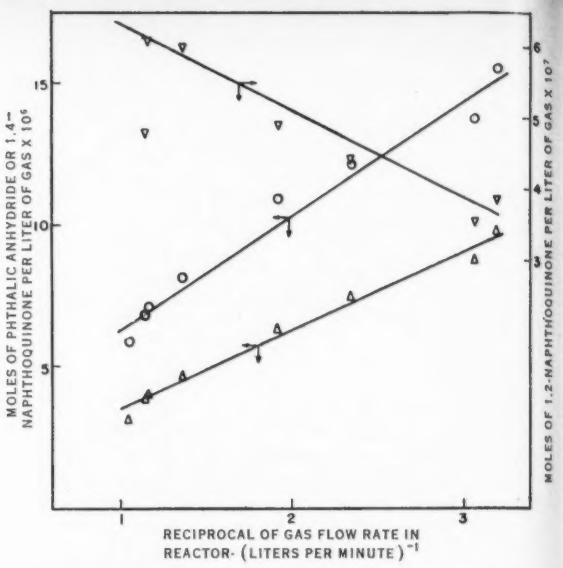

Figure 6—Variation with contact time of the concentration of 1,4-naphthoquinone (), phthalic anhydride (△), and 1,2-naphthoquinone (▽) in the gases leaving the bed of catalyst. Temperature 335°C. Oxygen concentration 6.6 x 10^{-3} moles per liter.

Comparison with Work Reported by Other Investigators

Calderbank[1] concluded that the rate of naphthalene oxidation is zero-order in the concentration of naphthalene. The present study shows this is so only for high naphthalene concentrations. In his plots of naphthoquinone formation, Calderbank[1] found an apparent conversion at W/F equal to zero. He concluded, therefore, that part of the naphthoquinone is formed by a homogeneous reaction. The experiments carried out by the present author in which no catalyst was present in the reactor (discussed above) have shown that the extent of this 'so-called' homogeneous reaction is much too small to account for the size of Calderbank's intercept. It is possible that the reaction products obtained by Calderbank contained a little 1,2-naphthoquinone which was not taken into account by his method of analysis. Since he used a colorimetric method to determine naphthoquinone, it is likely that his naphthoquinone analysis is too high due to the greater extinction coefficient of 1,2-naphthoquinone, and that this is the real reason why his plots indicated an intercept for W/F equal to zero. Calderbank[1] also concluded that 1,4-naphthoquinone and phthalic anhydride are formed by simultaneous reactions when the conversion of naphthalene is small. The present study agrees with this, with the modification that 1,2-naphthoquinone is an intermediate in the formation of phthalic anhydride from naphthalene.

Mars and van Krevelen[4] measured the rate of naphthalene conversion in a fluidized bed of catalyst. With this technique these authors were able to realize small naphthalene concentrations in the bed of catalyst. They observed that the reaction rate was dependent upon the concentration of naphthalene, as was also observed during the present study. These authors correlated their data using a kinetic equation identical in form with (3), based upon a model of the reaction involving an alternate reduction and oxidation of the catalyst surface.

Ioffe and Sherman[3] used an integral reactor in their study of this reaction. They found the reaction rate to be approximately first-order in the concentration of naphthalene at temperatures below 350°C. but that the specific rate constant on this basis decreased in value for an increase in the concentration of naphthalene in the feed gases. This anomalous behavior of the first-order constant is understandable in the light of the observations noted during the present study. Since the naphthalene concentrations used by Ioffe and Sherman[3] were relatively high it is probable that their reaction rate was more nearly zero-order than first-order in the naphthalene concentration. An increase in the concentration of naphthalene is then expected to result in a decrease in the value of the specific rate constant calculated as if the reaction were first-order in the naphthalene concentration.

In a second paper[9] devoted to a study of the products of the naphthalene reaction, Ioffe and Sherman concluded that a scheme of parallel and consecutive reactions was invloved. The present study is in agreement with this, with the modification that 1,2-naphthoquinone is an intermediate in the formation of phthalic anhydride from naphthalene.

D'Alessandro and Farkas[2] reported the oxidation of naphthalene to be first-order in the concentration of naphthalene. The present study agrees with this since these authors used low concentrations of naphthalene and high temperatures.

Conclusions

Rate data are reported for the oxidation of naphthalene under conditions resulting in low conversions. This has been correlated on the basis of a model proposed by Hinshelwood that a steady-state concentration of oxygen is established on

the catalyst surface. The resulting equation has also been shown to be consistent with the data in the literature.

It is shown that 1,2-naphthoquinone is formed in small amounts during the oxidation of naphthalene. This substance has not been reported by previous investigators of the kinetics of this reaction.

A scheme of parallel and consecutive reactions has been suggested for the course of the chemical reaction. In this scheme 1,4- and 1,2-naphthoquinone are intermediates in the formation of phthalic anhydride.

Acknowledgement

The authors are indebted to the Ontario Research Foundation and to the Advisory Committee on Scientific Research, University of Toronto, for financial support.

Nomenclature

C = gas concentration, moles per liter.
F = gas flow rate in reactor, liters per minute.
k_a = specific rate of adsorption of oxygen.
k_n = specific rate of reaction of naphthalene.
k_o = specific rate of reaction of adsorbed oxygen.
K_1 = equal to $(N\,k_n)/(k_a\,C_o)$.
K_2 = equal to $N/(k_a\,C_o)$.
N = moles of oxygen consumed per mole of naphthalene converted.
r = reaction rate, moles per gram of catalyst per second.
R = gas constant.
S = fraction of the catalyst surface covered with oxygen.
T = temperature.

Subscripts

n = naphthalene.
o = oxygen.

References

(1) Calderbank, P. H., The Industrial Chemist, 291, (1952).
(2) D'Alessandro, A. F., Farkas, A., J. Colloid Sci. **11,** 653, (1956).
(3) Ioffe, I. I., Sherman, J. H., Zhur. Fiz. Khim. **28,** 2095, (1954).
(4) Mars, J., van Krevelen, D. W., Chem. Eng. Science 3, (special supplement on the Proceedings of the Conference on Oxidation Processes) 41, (1954).
(5) Fieser, L. F., Org. Syntheses **17,** 68, (1937).
(6) Huntress, E. H., Mulliken, S. P., Identification of Pure Organic Compounds. John Wiley and Sons, Ltd., (1941). Page 148.
(7) Nagakura, S., Kuboyama, A., J. Am. Chem. Soc. **76,** 1003, (1954).
(8) Rosin, J., Rosenblum, H., Mack, H., Am. J. Pharm. **113,** 434, (1941).
(9) Hinshelwood, C. N., The Kinetics of Chemical Change. Oxford University Press, (1949). Page 207.
(10) Ioffe, I. I., Sherman, J. H., Zhur. Fiz. Khim. **29,** 692, (1955).

★ ★ ★

Oxidation of Ethylene Using Silver Catalyst Coated Strips in an Inert Fluidized Bed[1]

E. ECHIGOYA[2] and G. L. OSBERG[3]

Fluidized bed tests with silver catalysts used in the oxidation of ethylene to ethylene oxide showed fluidization instabilities due to catalyst agglomeration. One method of avoiding the agglomeration problem, yet utilizing the excellent heat transfer property of a fluidized bed, is by the immersion of fixed catalyst coated strips in an inert fluidized bed. Small scale tests with this method, have shown that excellent temperature control can be achieved without serious adverse effects on catalyst performance. Kinetic data are presented for a limited range of flow conditions, and are correlated by an empirical rate equation of the form

$$r = \frac{k\, p_e{}^m p_o{}^n}{1 + a\, p_{eo}}$$

The silver catalyzed oxidation of ethylene leads to the main overall reactions

$$C_2H_4 + 1/2\ O_2 \rightarrow C_2H_4O \quad \ldots\ldots\ldots\ldots\ldots\ldots (1)$$

$$C_2H_4 + 3\ O_2 \rightarrow 2CO_2 + 2H_2O \quad \ldots\ldots\ldots\ldots\ldots\ldots (2)$$

Large amounts of heat are evolved in this oxidation, particularly by reaction (2). Close catalyst temperature control is essential in order to achieve a maxiumum yield of ethylene oxide, and to maintain catalyst stability. One major requirement therefore of any practical reactor design suitable for these reactions is an adequate heat transfer rate.

The fluidized bed reactor would appear applicable because of its excellent gas-solid contact and its inherently high transfer rates. Its application has been hindered in part however by catalyst agglomeration effects[1] which cause fluidization instability. Packed tube reactors avoid agglomeration effects but have the disadvantage of relatively low heat transfer rates.

A combination of a fluidized and a fixed catalyst bed may however be an acceptable basis for a reactor design. Catalyst coated strips can be prepared from Ca Ag alloys[2] which are mechanically strong, and which can withstand the attrition effects of a fluidized bed. A bed material such as glass beads is inert in this reaction, and will serve as an excellent heat transfer medium. This combination should have some of the advantages of a fluidized bed such as high heat transfer rates, and easy catalyst replacement. It would have similar limitations on space velocity range, and would perhaps be less efficient in gas catalyst contact. Because of the novelty of the combination, and its potential application to the catalytic oxidation of ethylene, performance data were obtained on a small scale model reactor under a variety of process conditions.

[1]*Manuscript received February 4; accepted April 2, 1960.*
[2]*Tokyo Institute of Technology, Ookayama, Meguro-Ku, Tokyo, Japan.*
[3]*Division of Applied Chemistry, National Research Council, Ottawa, Ont.*
Contribution from Division of Applied Chemistry, National Research Council, Ottawa, Ont. Issued as N.R.C. No. 5685. Based on a paper presented to C.I.C. Chemical Engineering Conference, November 9-11, 1959.

Experimental

The reactor tube is shown schematically in Figure 1. It is made from 1½ in. I.D. × 28 in. stainless steel tube; with steel ball at the bottom of the conical bottom to act as a check valve. It is electrically heated, and the fluidized bed within it kept at a constant temperature by means of a temperature controller. Bed temperatures were recorded from thermocouples which passed through the wall and into the bed. The temperature difference between top and bottom bed thermocouples was about ± 2°C. Catalyst strip temperatures were not measured; so that temperature data in this report are based on the fluidized bed temperature.

The catalyst is sprayed on stainless steel strips which are attached to centrally located supporting structure, and is entirely immersed in the fluidized bed. The strips are arranged in four stages, each stage containing four strips spaced 90°C. apart, and rotated 45° with respect to one below it. The dimensions of a strip are 0.63 × 2.56 × .033 in. These strips were roughened by grit blasting, and passivated in a 50% nitric acid solution. The catalyst alloy (8.25% Ca 91.7% Ag) was put onto each side to a thickness of 0.02 in. by a flame spray method. Total weight of alloy on the sixteen strips was 37.6 gm.

The activated catalyst was obtained by steaming at 320° for 5 hours, followed by boiling in 20% acetic acid and water washing. The weight of activated catalyst remaining was 33.2 gm. Its residual calcium content was about 0.1% calcium; and its initial specific area was about 0.5 sq. m./gm. Following activation the catalyst was conditioned by operating the reactor for about two weeks. Its activity-time pattern during this period was similar to that reported by Orzechowski and MacCormack[3] except that a longer period was required to reach a constant level of activity. The data reported in this paper are based on performance after the two week conditioning period.

Glass beads, − 150 + 200 mesh, were used as the bed material. Other materials such as artificial graphite and silica were also tried. Artificial graphite caused minor catalyst poisoning, and formed dust. Silica gel dusted readily, and also catalyzed the isomerization of ethylene oxide to acetaldehyde. This isomerization could be eliminated however by treating the silica gel with 5 mole % sodium carbonate. Glass beads were superior to both these bed materials, since no poisoning occurred and elutriation was negligible.

Erosion of the catalyst surface by the fluidized glass bead bed was not a significant variable under the flow conditions tested. After the initial conditioning period catalyst activity

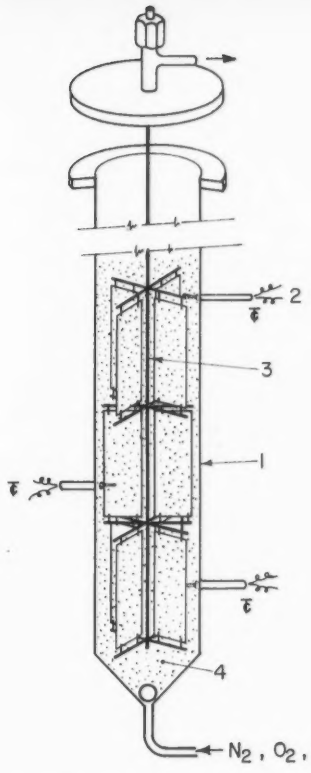

Figure 1—Mounting of catalyst strips in a reactor.

remained substantially constant over several weeks of continuous operation, which would not have occurred if appreciable amounts of catalyst were removed by erosion. Some erosion may have occurred but could not be detected by weighing the strips since glass beads had become embedded in the larger holes of the surface. Visual examination of strips at the end of the experiments did not reveal obvious wear.

The air was supplied to the reactor from a Nash Hytor compressor in which distilled water was used as the sealing fluid. Oxygen, nitrogen and ethylene were supplied from cylinders without further purification. Ethylene was obtained from Ohio Chemical Co. Limited, and was 99.5% purity. All feed gases to the reactor were metered with rotameters operating at 60 p.s.i.g.

Exit gases from the reactor passed through a cyclone, a pressure reducing valve, then a cooler, and finally a water bubbler, before being vented to an exhaust system. A sample of exit gas was taken from the line immediately ahead of the bubbler, and analysed for C_2H_4, C_2H_4O, and CO_2 by a gas chromatography method[4]. Accuracy of analysis for individual components was 1 - 2%. In experiments where low conversions were obtained, Drierite and Ascarite traps were placed in the inlet air line so as to reduce the possible error in product analysis caused by the presence of CO_2 and H_2O in the inlet air.

Correlation of Conversion Data

Conversion data as a function of W/F ratios were obtained at constant fluidized bed temperature and at constant air to ethylene ratios. The ratio W/F was varied by holding F constant and varying W, i.e. by mounting two, three or four sets of catalyst strips in series within the fluidized bed. The flow rate was set at about three times the minimum required for fluidization. An alternate method of changing W/F is holding W constant and changing F. The range of gas flow is limited to the range between minimum fluidization and the onset of severe slugging. When slugging occurred, large gas bubbles uncovered the catalyst causing poor heat transfer, and so uncontrolled catalyst temperature. Within the gas flow range of good fluidization, adequate temperature control was obtained. Conversion data at the same W/F ratios were not significantly different between the two methods of changing W/F ratios.

Ethylene Dependence

Conversion data based on variable W and constant F are listed in Table 1, where x is the fraction of ethylene feed which has been oxidized to all products, and selectivity, S, is the fraction of the total ethlene consumed which has been oxidized to ethylene oxide. Plots of the data at several bed temperatures with an air-ethylene ratio of 15:1 are given in Figure 2. Similar plots were made with air-ethylene ratio of 20:1 and 35:1. Initial rates were obtained by drawing tangents to best fitting curves at $W/F = 0$, and these slopes were replotted as log r_o against log p_e. Linear plots were obtained at each temperature having a common slope of 0.5, so that the initial rate data may be represented by the empirical Equation (3).

$$r_o = k_1 p_e^{0.5} \quad \ldots\ldots (3)$$

It was assumed that the oxygen concentration was substantially constant, though in fact it varied from 19.6 to 20.3% in the feed. This variation is not sufficient to affect the rate significantly. The average values of k_1 at each bed temperature are summarized in Table 1.

An activation energy for the overall oxidation of ethylene of 12.9 K. cal./mole was obtained by the usual methods.

Oxygen Dependence

The dependence of the overall oxidation rate on oxygen was obtained at constant W/F, and at constant ethylene concentration by varying oxygen to nitrogen ratio. Data are listed in Table 2, along with the initial rates as calculated directly from the conversion data. When log xyF/W was plotted against log p_o, substantially linear plots were obtained with slopes of 0.23, 0.27 and 0.24 at 237, 250, and 270°C. respectively. Using an average value of 0.25 for the slope, and combining this result with Equation (3), the initial rate of overall ethylene consumption is expressed as

$$r_o = k_2 p_e^{0.5} p_o^{0.25} \quad \ldots\ldots (4)$$

From the data in Tables I and II, k_2 has been evaluated at each temperature, so that at $p = 1$ atm. it is given by

$$k_2 = 6.64 \times 10^3 \, e^{\frac{-12{,}900}{RT}} \quad \ldots\ldots (5)$$

Effect of Total Pressure

Data for the pressure range up to 4.5 atmosphere are listed in Table III. Cylinder nitrogen, and oxygen were used in place of air in these experiments. Some of the data are plotted in Figure 3, showing that at constant W/F, total conversion, x, increased rapidly, then more slowly as the total pressure was increased.

Observed rate data at finite conversions are lower than would be predicted by Equation (4). This is due in part to the inhibiting effect of the products on the reaction rate. Hayes[3] has shown that CO_2 inhibits the rate of oxidation of ethylene to ethylene oxide with no significant effect on the rate of oxidation of ethylene to carbon dioxide and water. He reports no apparent effect on either reaction rate when water vapor is added with inlet gas. Kurilenko et al.[6] however found that all three products inhibit both main reactions. The order of decreasing inhibiting strength is given as ethylene oxide, carbon dioxide and water. The inhibiting effects of products and the effect of total pressure were taken into account by correlating the data with an equation of the form

$$r = \frac{k_2 p_e^m p_o^n}{1 + a p_{co}} \quad \ldots\ldots (6)$$

TABLE 1

CATALYTIC OXIDATION OF ETHYLENE WITH AIR AT P = 1 ATM.

Bed Temp.			239°C.		250°C.		257°C.		269°C.	
W gm.	W/F*	Air/C_2H_4	x	S	x	S	x	S	x	S
16.6	0.85	35:1	.075	.54	.084	.56	.092	.53	.123	.52
24.9	1.27	35:1	.077	.56	.121	.54	.148	.53	.178	.52
33.2	1.70	35:1	.114	.55	.134	.60	.167	.54	.198	.52
		10^3r_0	2.34		2.90		3.62		4.45	
16.6	0.83	20:1	.053	.53	.071	.53	.078	.54	.111	.53
24.9	1.25	20:1	.078	.54	.093	.54	.112	.53	.149	.54
33.2	1.67	20:1	.086	.57	.094	.57	.128	.54		
		10^3r_0	3.14		3.81		4.66		6.39	
16.6	0.82	15:1	.045	.58	.053	.51	.064	.52	.088	.53
24.9	1.23	15:1	.065	.55	.084	.54	.105	.54	.132	.56
33.2	1.64	15:1	.072	.56	.102	.55	.108	.57	.158	.56
		10^3r_0	3.50		4.37		5.37		7.12	
	Mean	10^2k_1	1.41		1.74		2.15		2.81	

*W/F = gm Ag catalyst/mole/hr. of total gas flow
r_0 = mole C_2H_4 consumed/hr.−gm.Ag.

The choice of p_{co} as a correlating variable is arbitrary. Since the selectivity values in this group of data is in a narrow range 52 - 60, the partial pressure of carbon dioxide or even the sum of products may be just as suitable.

An integrated form of this empirical rate equation was used for evaluating α. It was obtained by substituting Equation (6) in the flow Equation (7) for piston flow.

$$W/F = y\int_0^x \frac{dx}{r} \qquad (7)$$

With the following substitutions for partial pressures,

$$p_e = py\,(1 - x)$$
$$p_e = py\,(a - 3x + 5/2\,Sx)$$
$$p_{co} = pyxS$$

and assuming the partial pressure of oxygen to be constant, the resulting expression (8) is obtained.

$$W/F = e\,(X + cY) \qquad (8)$$

where $X = 2\,(1 - \sqrt{1 - x})$

$$Y = 2/3\,[2 - (2 + x)\,(1 - x)^{1/2}]$$

TABLE 2

EFFECT OF VARYING PARTIAL PRESSURE OF OXYGEN ON OXIDATION OF ETHYLENE

Bed Temp.	0_2	N_2	$C_2H_4(y)$	x	S	$\frac{xyF}{W}$
°C.	—	atm.−				10^{-3}
237	.187	.750	.063	.072	.58	2.76
	.374	.561	.063	.085	.58	3.26
	.561	.374	.063	.088	.60	3.38
250	.187	.750	.063	.093	.57	3.57
	.374	.561	.063	.110	.58	4.22
	.561	.374	0.63	.129	.59	4.95
270	.187	.750	0.63	.143	.54	5.50
	.374	.561	.063	.165	.56	6.34
	.561	.374	.063	.180	.56	6.92

$W/F = 1.64\ \frac{\text{gm.}-\text{hr.}}{\text{mole}}$ W = 33.2 gm.

$$c = \alpha\,spy$$

$$e = \frac{y^{1/4}}{k_2 p^{3/4}\,a^{1/4}}$$

The constant α may be calculated by substitution of the experimental values shown in Table 3 into Equation (8). The calculated values of α are shown in Table 3. These values were plotted as log α vs $1/T$, and show considerable scatter, but a definite trend with temperature. By the method of least squares a best fit line was calculated as:

$$\log \alpha = -2.084 + \frac{2.16 \times 10^3}{T} \qquad (9)$$

TABLE 3

CATALYTIC OXIDATION OF C_2H_4 AT VARIOUS TOTAL PRESSURES

Bed Temp. °C.	Press atm.	x	S	α equ'n(8)	α equ'n(9)	x calc.
232	2.36	.083	.58	155		.082
	3.38	.086	.60	167	156	.088
	4.46	.100	.62	113		.090
237	1.0	.072	.58	164		.073
239	1.68	.086	.56	158		.089
	2.36	.093	.60	157	134	.097
	3.44	.098	.60	160		.105
	4.46	.104	.61	147		.108
242	2.36	.098	.59	170		.108
	3.38	.109	.60	151	128	.120
	4.53	.127	.59	115		.121
250	1.0	.093	.57	111		.090
	1.82	.123	.57	93	113	.117
	2.36	.130	.59	98		.124
	3.38	.142	.60	93		.132
	4.46	.148	.62	90		.138
	4.53	.154	.60	87		.139
257	1.0	.115	.55	87		.113
	1.68	.133	.55	118		.142
	2.36	.153	.56	100	97	.155
	3.44	.171	.58	89		.168
	4.60	.181	.58	86		.175
270	1.0	.143	.54	99		.148
	2.36	.200	.55	78	77	.200
	3.44	.210	.56	83		.213
	4.60	.220	.56	74		.220

*$W/F = 1.64\ \frac{\text{gm.hr.}}{\text{mole}}$
W = 33.2 gm.
$C_2H_4:O_2:N_2$ = 1:3:12

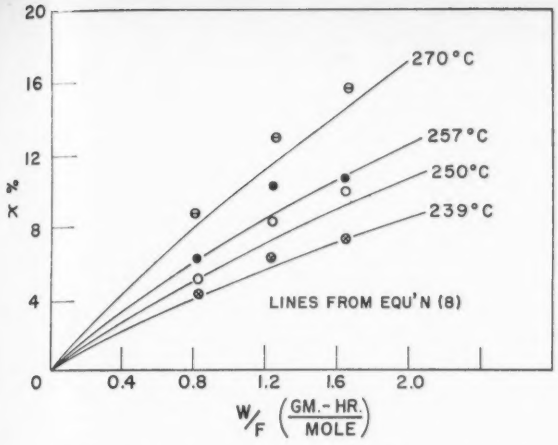

Figure 2—Total conversion of C_2H_4 vs W/F at several temperatures and constant air:C_2H_4 ratio 15:1.

Calculated values of α from Equation (9) are given in Table 3. These values of α, along with the empirically determined values of m, n and k_2 were used to calculate the conversion x. Conversion values in Table 3, and the solid lines drawn in Figures 2 and 3 which were calculated from Equation (8) show satisfactory agreement with the observed data.

Selectivity

The selectivity of the catalyst showed the usual trend noted by previous authors[7]. Selectivity increased slightly with increasing partial pressure of oxygen, and decreased with increasing catalyst temperature. Data illustrating the trend with temperature have been plotted in Figure 4. Values of selectivity were taken from this best fit line in calculating the conversion curves shown in Figures 2 and 3.

Discussion of Results

The power law form of the rate equation was chosen because of its simplicity. Equations proposed from mechanistic considerations did not fit these data too well. For example, Kurilenko's et al.[6] equation predicted no dependence on oxygen concentration whereas these data showed some dependence. Orzechowski and MacCormack's Equation (3) which fit their data (at $p = 1$ atm) on a similar catalyst was not fully applicable to this group of data. Their equation for initial rate can be written in the form

$$\frac{1}{r_o} = \frac{1}{k} + \frac{1}{kp}\left(\frac{a}{y} + \frac{b}{y_o}\right) \quad \ldots\ldots\ldots\ldots\ldots\ldots (10)$$

Initial rate data given in Table 1 from experiments at atmospheric pressure fitted Equation (10) and thus were in agreement with

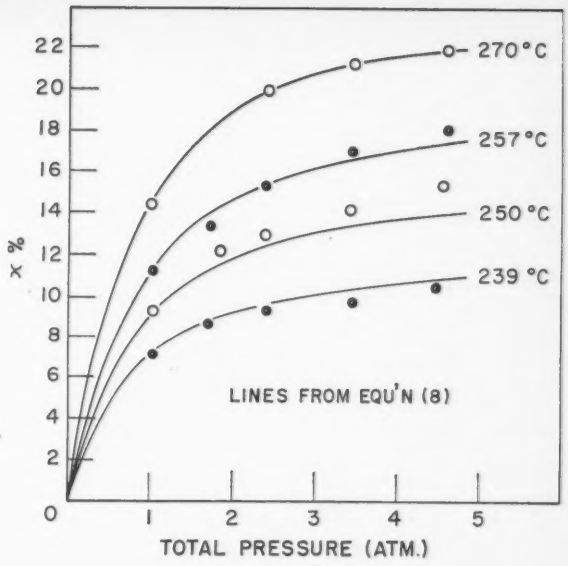

Figure 3—Total conversion of C_2H_4 vs total pressure at constant W/F = 1.64; air: C_2H_4 ratio 15:1.

the earlier work[3]. This equation also predicted satisfactorily the functional dependence of initial rate on total pressure, but the constant k which can be obtained from the intercept of plot $1/r_o$ vs $1/p$, was from 1/3 to 1/18, depending on the temperature, the value of k derived from the data at atmospheric pressure. Thus constants k, a and b at the higher pressures were not consistent with the constants obtained at p equal to one; and appear to be functions of total pressure as well as temperature.

Power law forms of the rate equation have been applied to this reaction. Cambron and McKim[7] found that the overall ethylene consumption to be proportional to $p_e^{0.5}$ which is in agreement with the data reported here. Shen-Wu[8] correlated his data with the equation

$$r = k' p_e^{0.365} p_o^{.667}$$

Thus, exponents of p_e and p_o vary in magnitude and seem to depend on catalyst preparation and conditions under which the catalyst has been tested.

The activation energy obtained from the overall oxidation of ethylene in these tests is 12.9 K. cal./mole. This value is somewhat lower than given by Kurilenko et al.[6] who reported 15.2 and 19.8 K. cal. for reactions (1) and (2) respectively. The reason for the lower activation energy is not known, though it might possibly be due to the onset of diffusion effects. A rough estimate of the eddy diffusivity coefficient within the

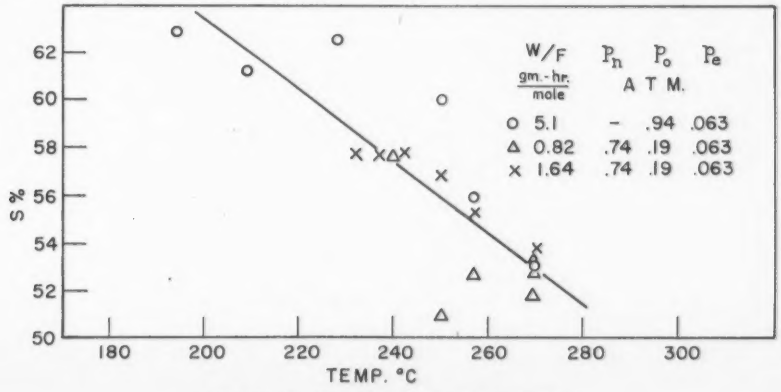

Figure 4—Selectivity vs temperature.

fluidized bed using Gilliland and Mason's data[9] indicated that no significant radial concentration gradient should appear for the reaction rates observed. An estimate of the back mixing effect using the same data, also showed that back mixing should have only a minor effect on the conversion levels. The diffusion effects within the catalyst film itself are believed to be small but could not be satisfactorily evaluated because effective diffusivity data for the catalyst film were not available.

A comparison of observed catalyst activity with data derived from catalyst coated tubes similar to those used by Hayes[5] showed that under comparable operating conditions, the activity was substantially the same, but that selectivity may be slightly lower. Selectivity is significantly lower when compared with Hayes' data where conditions were not identical. Hayes used lower flow rates, and carefully purified feed gases.

These experiments have shown that the immersion of fixed strips in an inert fluidized bed is a feasible method of obtaining close temperature control without appreciable loss in catalyst performance. Moreover, the method permits easy catalyst replacement when it becomes necessary. An obvious limitation, which is common to fluidized bed systems, is the limitation on maximum flow rate, which thus restricts the space velocity to relatively low values. This maximum flow rate is set by the flow at which severe slugging develops. The scale up factors which affect this limit have not yet been determined.

Summary

Small scale experiments have shown that close temperature control without reduction in catalyst activity can be obtained by immersing catalyst coated strips in an inert fluidized bed.

Rate data obtained from the air oxidation of ethylene using immersed Cambron silver catalyst coated strips in a glass bead bed were correlated by the empirical equation

$$r = k_2 \frac{p_e^{1/2}\, p_o^{1/4}}{1 + \alpha\, p_{eo}}$$

Constants have been evaluated for variables in the range T-230-270°C., p-0-50 p.s.i.g.; air/C_2H_4 ratio 35/1 to 15/1; O_2 concentration −20 −56%. The constants k_2 and α for this range of data are:

$$\log_{10} k_2 = +3.822 - \frac{2.80 \times 10^3}{T}$$

$$\log_{10} \alpha = -2.084 + \frac{2.16 \times 10^3}{T}$$

Acknowledgement

We are indebted to D. Kulawic for the chemical analysis of products; and G. Despault for other technical assistance.

Nomenclature

a	=	oxygen to ethylene ratio
c	=	α Spy
e	=	$\dfrac{y^{1/4}}{p^{3/4}\, a^{1/4}\, k_2}$
F	=	total gas flow − mole/hr.
k_1, k_2	=	empirical rate constants − $\dfrac{\text{mole}}{\text{hr.} - \text{gm.} - \text{atm.}^{1/2}}$ $\dfrac{\text{mole}}{\text{hr.} - \text{gm.} - \text{atm.}^{3/4}}$ resp.
m, n	=	empirical exponents − 1/2 and 1/4 resp.
p_e, p_o, p_{eo}	=	partial pressure of ethylene, oxygen, ethylene oxide, resp., atm. in inlet gas stream.
p	=	total pressure − atm.
$r_o, r,$	=	initial rate, and rate of C_2H_4 consumed in − mole/hr. − gm. catalyst
R	=	gas constant
S	=	selectivity
T	=	temperature °K
W	=	weight of silver catalyst − gm.
x	=	fraction of inlet ethylene converted
y, y_o	=	mole fraction of ethylene, oxygen in feed
α	=	empirical constant − atm.$^{-1}$

References

(1) Echigoya, E., Osberg, G. L., Can. J. Chem. Eng. **38,** 43 (1960).

(2) Cambron, A., McKim, F. L. W., U.S. Pat. 2,562,857, (1951) Can. Pat. 475,366 (1951).

(3) Orzechowski, A., MacCormack, K. E., Can. J. Chem. **32,** 388, (1954).

(4) Amberg, C. H., Echigoya, E., Kulawic, D., Can. J. Chem. **37,** 708, (1959).

(5) Hayes, K. E., submitted. Can. J. Chem.

(6) Kurilenko, A. I., Kul'Kova, N. A., Rybakova, N. A., Temkin, M. I., Zhur. Fiz. Khim. **32,** (4) 797-805 (1958).

(7) McKim, F. L. W., Cambron, A., Can. J. Research **27B,** 813 (1949).

(8) Shen-Wu Wan, I.E.C. **45,** 234, (1953).

(9) Gilliland, E. R., Mason, E. A., I.E.C. **41,** 1191 (1949).

★ ★ ★

Evaporation Rates in Spray Drying[1]

J. DLOUHY[2] *and W. H. GAUVIN*[2]

Heat and mass transfer coefficients have been determined during the evaporation of water sprays produced by pneumatic atomizing nozzles in a vertical, cocurrent spray dryer, 8-in. in diameter and 14 ft. high, under various operating conditions. The progressive evaporation of the spray down the chamber was followed by taking samples of the drying air and of the water droplets at various distances from the nozzle, and a new volumetric method for the accurate determination of air humidities was developed.

For droplet spray ranging in mean diameter from 11.5 to 38.5 microns, the heat and mass transfer coefficients were found to be essentially the same as for single, stationary droplets evaporating in still air, the similarity being attributed to the almost equal diffusivity of the drop and of the air stream, resulting in negligible relative velocity. Certain important aspects of spray dryer design are discussed, and a method is outlined for the calculation of the residence time in the evaporation zone.

Les auteurs ont déterminé les coefficients de transport de chaleur et de masse durant l'évaporation d'eau en jets pulvérisés produits par des atomiseurs pneumatiques, dans un séchoir à jet vertical concourant, de 8 pouces de diamètre par 14 pieds de hauteur. Ils ont suivi l'évaporation progressive du jet le long de la chambre en prélevant des échantillons d'air et de gouttelettes d'eau à des distances variées de l'atomiseur. On a mis au point une nouvelle méthode volumétrique pour déterminer avec précision l'humidité de l'air.

Les auteurs ont trouvé que pour des gouttelettes ayant des diamètres variant entre 11.5 et 38.5 microns, les coefficients de transport de chaleur et de masse sont essentiellement les mêmes que pour des gouttelettes uniques et stationnaires qui s'évaporent dans de l'air au repos. On attribue ces comportements semblables aux diffusivités très voisines de la gouttelette et du courant d'air, donnant une vitesse relative négligeable. On présente certains aspects importants de la réalisation de séchoirs à jets pulvérisés et on décrit une méthode pour le calcul du temps de résidence dans la zone d'évaporation.

The drying chamber of a conventional spray dryer may be considered as consisting of three distinct zones, namely the nozzle zone, in which the newly-atomized drops rapidly decelerate to their final settling velocity, the evaporation zone, in which the mechanism of water vapor evolution is similar to that from a free liquid surface, and finally the drying zone, in which internal diffusion in the drying particles becomes the governing factor. The present investigation was undertaken to determine the rate of heat and mass transfer to the drops in the evaporation zone under conditions likely to be encountered in spray dryers.

1. Evaporation from Single Particles

In 1910, Morse[1] showed experimentally that the rate of evaporation from a stationary drop in a gas was proportional to its diameter. His results were analyzed by Langmuir[2] who presented the following theoretical equation:

$$-dm/d\theta = s \int D_v \, d\rho_v \qquad (1)$$

in which the factor s accounted for the thickness of the film surrounding the drop, through which diffusion of the vapor occurred, and was defined by:

$$s = 4\pi r_o r_b/(r_b - r_o) \qquad (2)$$

Equation (1) was verified by many workers experimentally and it was modified by others to take into account certain specific conditions. In particular, Fuchs[3] made a correction for the concentration of the diffusing vapor at an infinite distance from the drop, and Froessling[4] added a term to take into account the relative velocity between the gas and the drop. His equation was based on an approximate solution of the Navier-Stokes equations but included experimental coefficients, and can be written as follows:

$$Nu' = 2.0 + 0.552(Re)^{1/2}(Sc)^{1/3} \qquad (3)$$

Several other forms of this equation were suggested, and in 1952 Ranz and Marshall[5], following an extensive study, presented the following four equations for heat and mass transfer to a drop under natural or forced convection:

$$Nu = 2.0 + 0.60(Re)^{1/2}(Pr)^{1/3} \qquad (4)$$

$$Nu' = 2.0 + 0.60(Re)^{1/2}(Sc)^{1/3} \qquad (5)$$

$$Nu = 2.0 + 0.60(Gr)^{1/4}(Pr)^{1/3} \qquad (6)$$

$$Nu' = 2.0 + 0.60(Gr)^{1/4}(Sc)^{1/3} \qquad (7)$$

[1]*Manuscript received October 6, 1959; accepted March 30, 1960.*
[2]*Pulp and Paper Research Institute of Canada and Department of Chemical Engineering, McGill University, Montreal, Que.*

At high rates of evaporation – which may occur with elevated drying air temperatures or when the liquid has a low latent heat of vaporization – the diffusing vapor leaving the drop surface changes the temperature gradient in the gas film surrounding the drop, and the *apparent* values of the Nusselt Number given by Equations (4) and (6) are too high. To get the *actual* value of Nu, use of a correction gas been recommended by several workers[6,7,8,9,10].

2. Evaporation from Clouds of Particles

Although the same theoretical considerations apply to clouds of drops as for single drops, the problem is complicated by the fact that, in a spray dryer, the drops are dispersed in a turbulent gas stream. Liu[11] and Soo[12] studied theoretically the forces acting on single particles suspended in a turbulent gas and their results indicated that the eddy diffusivities of the particles and of the gas are almost equal for small particles and at low intensities of turbulence. This means that the drops should evaporate at a rate corresponding to zero relative velocity.

Kesler[13] studied experimentally the diffusion of atomized sprays in turbulent air streams. The work was carried out in a 44-ft. long duct (5.76-in. I.D.), with air velocities ranging from 25 to 90 feet per second, and Kesler found that the diffusion coefficients of water and alcohol drops ranging from 14 to 30 microns in diameter were approximately equal to that of the air. He also found that the rate of evaporation of 25-micron alcohol drops was equal to the predicted rate for stagnant conditions and therefore concluded that the relative velocity between the drops and the air stream was essentially zero.

A few studies have been reported on the rate of evaporation under decelerating or accelerating conditions in the nozzle zone of a spray dryer[14] and particularly in the field of fuel atomization[15,16,17]. Most of the data give fair agreement with Equation (4), but the high relative velocities between the drop and the air tend to mask any effects due to air turbulence and the results cannot be readily applied to the evaporation zone of a spray dryer.

Experimental

In conventional spray dryers the particle trajectories and gas flow patterns are invariably quite complex, and it is therefore impossible to follow the progressive evaporation of the droplets. Following the approach initiated by Pinder[18], a special vertical cocurrent spray dryer was therefore designed, permitting the simultaneous determination of the air temperature and humidity, as well as the droplet size distribution as evaporation proceeded, thus enabling the calculation of heat and mass transfer coefficients along the drying chamber.

1. Equipment

The experimental spray dryer consisted of the same basic units as an industrial installation, except that no device for product collection was provided.

The drying chamber was 14-ft. long, 8-in. in diameter, and was insulated with a 2-in. layer of vermiculite. Sampling ports were provided along the whole length of the chamber, as shown in Figure 1.

Two blowers were used, one at each end of the unit and both equipped with a sliding gate, so that the air rate and pressure in the drying chamber could readily be controlled. A calibrated orifice was used to meter the drying air and a perforated plate was installed at the top of the chamber to provide a uniform air distribution. Three electric heaters with a total capacity of 6.25 kw.

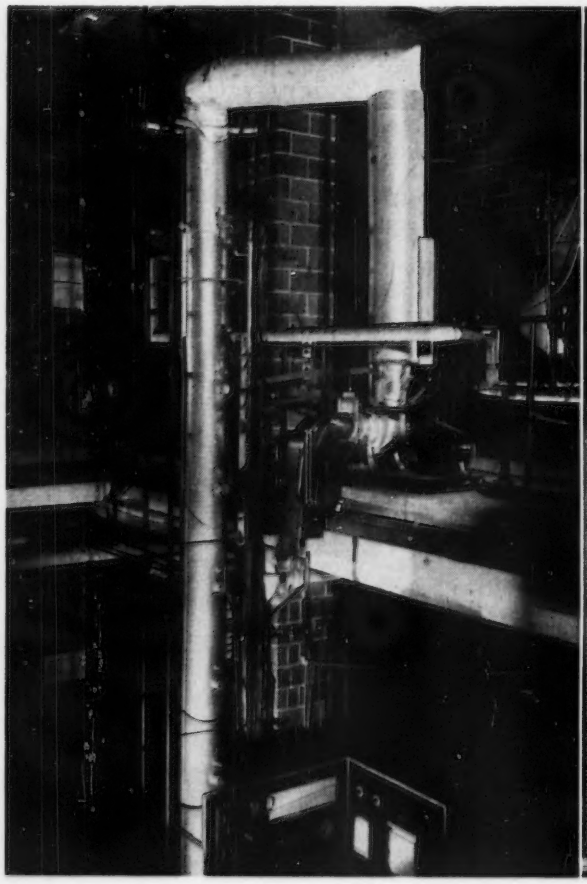

Figure 1—Experimental spray dryer.

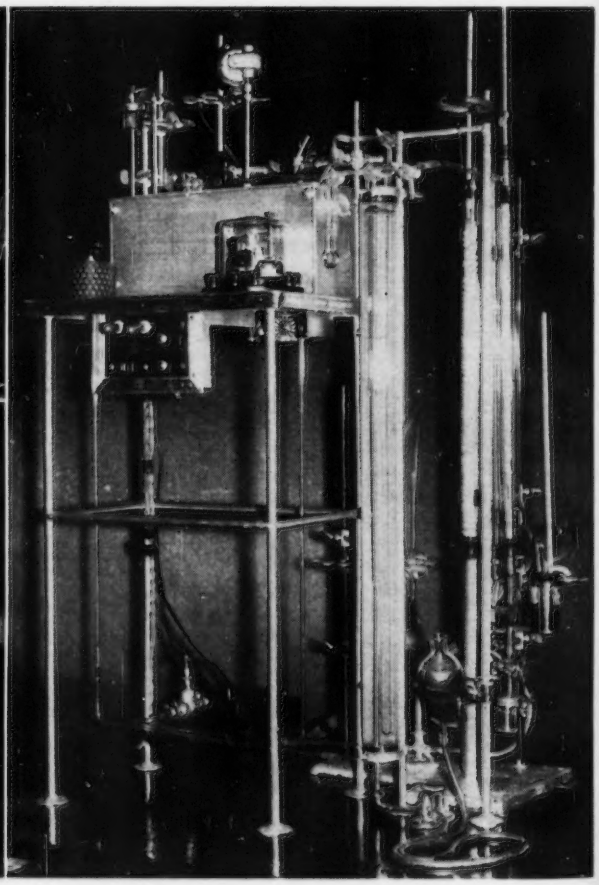

Figure 2—Humidity determination apparatus.

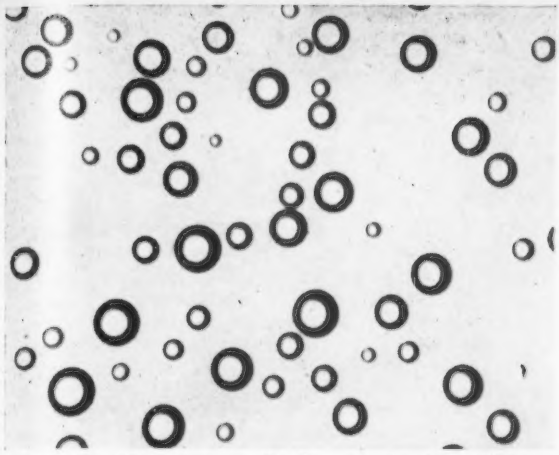

Figure 3—Photomicrograph of water droplets (220x).

supplied the necessary heat. A variac and an Aminco bimetallic thermoregulator assured fine control of the air temperature and a Speedomax 12-point potentiometer recorder was used to measure the inlet and outlet air temperatures as well as the wall temperatures at various points in the drying chamber to indicate when steady state conditions were established in the system.

An internal-mixing pneumatic nozzle (supplied by the Spraying Systems Company) was installed in the center and at the top of the drying chamber. Two different sizes were used, (Models No. 12 and 22B), both with a spray angle small enough to insure that the droplets did not impinge on the walls of the drying chamber under the conditions studied. The liquid feed to the nozzle consisted of tap water metered through a rotameter and heated or cooled in a heat exchanger just before entering the nozzle. Instruments were provided to indicate the atomizing air and liquid feed pressures, as well as the feed temperature.

All valves, instruments and controls were mounted on a central control panel, a portion of which can be seen at the bottom of Figure 1.

2. Methods of Measurement

(a) Air Temperature

The presence of liquid droplets in the air stream necessitated the use of a special shield to protect the temperature measuring device. After considerable experimenting it was found that a semi-circular shield, 0.4-in. in diameter and 1.5-in. long, protecting a mercury thermometer bulb 0.2-in. in diameter, was most suitable. By spraying colored solutions into the chamber any droplet impingement on the bulb could be observed after withdrawing the thermometer and it was found to be negligible. Conduction losses along the stem were reduced by installing the thermometer in a glass tube.

(b) Air Humidity

Owing to the small changes in drying air humidity observed in this investigation, a considerable degree of accuracy was required for the humidity measurements. The majority of the more conventional methods were found to be either insufficiently accurate or unsuitable because of a large air sample requirement. A volumetric method of determining the humidity of the air was therefore developed, based on the absorption of water vapor by magnesium perchlorate (which does not absorb carbon dioxide or any other common gases) under constant temperature and pressure conditions, and on the accurate measurement of the resulting change in the volume of the air sample.

A precision Mine Air Gas burette of 100-ml. capacity, calibrated in 0.05-ml. subdivisions in the range 94-100 ml., was used to measure changes in volume of the air as low as 0.01-ml. after it was passed over magnesium perchlorate in a U-tube. From the burette the air could be passed through the U-tube and into a self-sealing mercury reservoir, consisting of two interconnected chambers, mounted one above the other. The air entering the lower compartment forced the mercury into the upper section. When the air was sucked back into the burette, the mercury flowed back into the lower chamber. A fixed level of mercury in the lower chamber was obtained by means of a pilot-light circuit with contacts sealed into the mercury chamber. Three passes were found to be required for complete removal of the water vapor.

A constant temperature water bath, and a jacket around the burette with water circulating from the bath through it, wer used to maintain rigidly constant temperatures throughout th system, while a compensator tube and manometer ensured constant reference pressure. A photograph of the apparatus i shown in Figure 2.

The whole method depended on the assumption that the volume of the magnesium perchlorate did not change during a test so that the volume of dry air trapped in the U-tube was the same for the initial and final measurements. This assumption was undoubtedly justified in view of the small amounts of water which were absorbed, but the equipment was calibrated to ensure reliable results. Air of a known humidity was prepared by saturating it at a given temperature in two absorption columns which can be seen on the right in Figure 2. Calibration tests indicated that the method was accurate within 0.78% in the range 0.0118 to 0.0150 lb. water/lb. air.

Air samples were obtained from the chamber by employing an inverted cup, 0.75-in. I.D., which was inserted into the drying chamber and through which air was sucked into an evacuated sampling bottle. The rate of suction was such that the air velocity in the cup was well below the average terminal velocity of the drops, thus achieving the desired separation. An aluminum lip on the periphery of the cup prevented the collected spray from entering the sampling device.

(c) Droplet Size

Since the rate of evaporation is a function of the droplet diameter, it was necessary to determine the particle size distribution at various locations in the drying chamber. The microscopic method, being direct, was chosen in this investigation.

Samples of the spray were collected in an immersion cell filled with Varsol, similar to that described by Rupe[19], to prevent evaporation of the droplets before they could be photographed. The immersion cells (0.18-in. I.D. and 0.25-in. O.D.) were made small to minimize deflection of the small particles, and a piece of optical glass, coated with General Electric SC. 87 "Dri-film" was cemented into the bottom of the cells. Rupe has shown that, employing the above precautions, the drops remain spherical and their diameter can therefore be measured directly. Furthermore, the low surface tension between Varsol and water keeps coalescence between the drops to a minimum. Good target efficiencies were obtained with these small cells, as evidenced by the large number of small drops (down to 1 μ) collected.

The sample obtained from a traverse of the spray was immediately photographed through a microscope with 54.3× magnification using a single lens reflex camera and high resolution film (Adox KB-14, 141 lines per mm.). High contrast prints were obtained from the negatives and these were viewed and counted under low (43×) magnification through a microscope. Several hundred drops were measured from each sample and grouped into sizes separated usually by 2.38 microns. A typical photomicrograph of water droplets is shown in Figure 3.

3. Procedure

A series of runs was made to determine the rate of evaporation of the water droplets under various experimental conditions, according to a rigidly standardized operating procedure.

After selecting the proper air temperature and air rate, the system was allowed to reach steady state conditions. No feed was introduced to the nozzle at this stage, but atomizing air

was passed through at the desired pressure. A temperature traverse of the air along the length of the drying chamber was then made to determine the heat losses and to correct for the presence of the cold atomizing air. It was invariably found that the heat loss was negligible, but that the correction for atomizing air was necessary – the corrected inlet air temperature thus obtained was designated by t_o.

Water was then introduced at the nozzle and once again time was allowed for steady state to be reached. Special precautions were taken at this stage to ensure that the spray did not impinge on the chamber walls as shown by observation of the wall temperatures and physical inspection of the walls with proper lighting.

The feed, atomizing air and inlet drying air conditions and rates were noted and the temperature and humidity distribution along the drying chamber were determined as described previously. Droplet size distributions were also obtained at selected distances from the nozzle. It was ascertained, by means of an unshielded thermocouple probe, that in all runs the water droplets remained at the wet bulb temperature of the air throughout the chamber.

4. Calculations

The rate of evaporation of the water droplets was calculated directly from either a heat balance or a material balance. For the accurate calculation of the instantaneous heat transfer coefficients, however, an equation had to be derived on a differential basis because of the continuous variation in the values of the variables involved in the system. Considering a height dx of the chamber, the following heat balance can be written:

$$-wc_s dt = wdH\,[\lambda_w + C_{pv}(t - t_w)] \quad \ldots\ldots\ldots\ldots (8)$$

while the rate of heat transfer to the drops located in the differential volume of the chamber of height dx is given by:

$$w\lambda_w dH = h(t - t_w)dA \quad \ldots\ldots\ldots\ldots\ldots\ldots (9)$$

dA, the surface area of the droplets can be obtained from S_w, the specific area of the spray (in ft.²/lb. of water), by means of the expression:

$$dA = \left[\frac{S_w L}{V_a + V_t}\right] dx \quad \ldots\ldots\ldots\ldots\ldots\ldots (10)$$

In Equation (10) the terminal velocity of the droplets, V_t, is considered to be negligible in comparison with the absolute velocity of the air, V_a. In the actual experiments, V_t varied from 10^{-2} to 10^{-1} ft. per sec., depending on the drop diameter. L, the pounds of unevaporated liquid droplets passing per hour through the cross-section in question, was calculated from the water feed rate at the nozzle by means of a humidity balance, and S_w was obtained from the droplet count at the section by substitution into the following expression:

$$S_w = 6\Sigma nd^2/\rho\Sigma nd^3 = 6/\rho d_{vs} \quad \ldots\ldots\ldots\ldots\ldots\ldots (11)$$

From these equations, the instantaneous values of h could be readily calculated. These are the actual values from which the actual Nusselt Numbers, $Nu = (hd_{vs}/k_f)$, can be obtained. The latter can be compared directly with the apparent values predicted by Equation (4) since the drying air temperatures (maximum 229.7°F.) were low, and the correction for high mass transfer rate consequently negligible.

From similar equations and from their definition, the instantaneous mass transfer coefficients, k_G, and the modified Nusselt Numbers for mass transfer, Nu′, were calculated.

It is to be noted that the mean film properties such as μ_f, ρ_f, k_f, were estimated at the arithmetic average temperature between the air and the surface of the droplet, or the air wet bulb temperature.

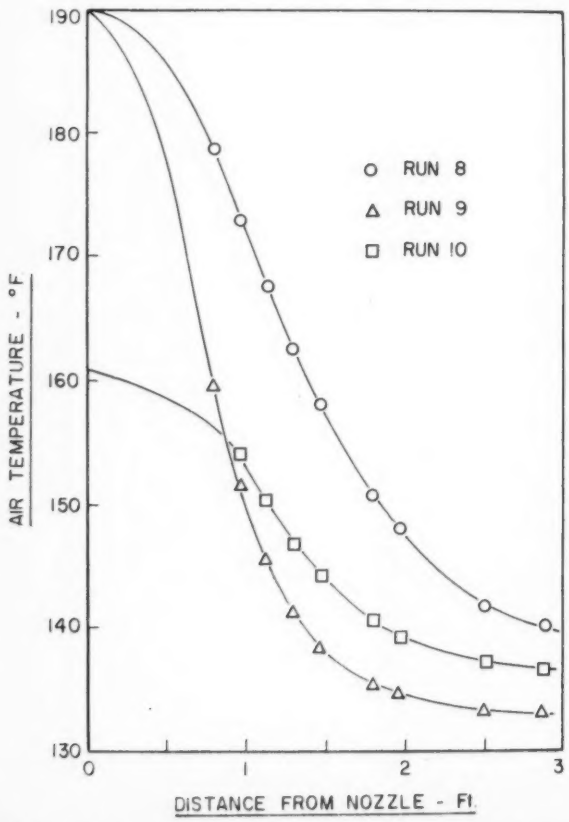

Figure 4—Typical temperature distribution in spray dryer.

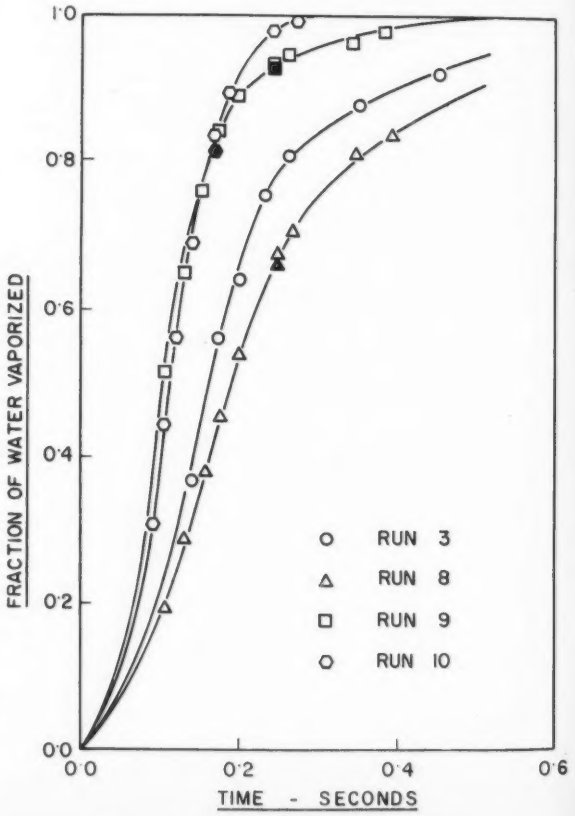

Figure 5—Rate of water vaporization.

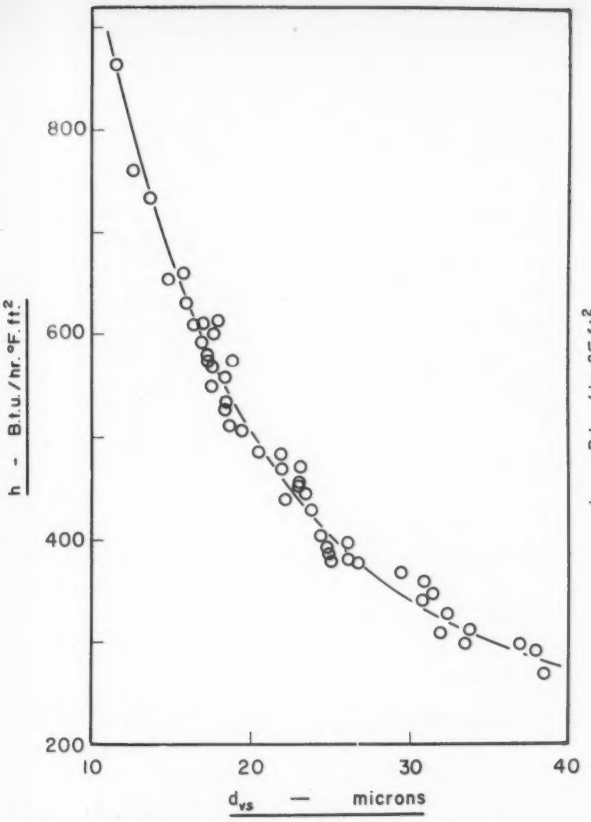

Figure 6—Variation of heat transfer coefficient with mean statistical droplet diameter, d_{vs}.

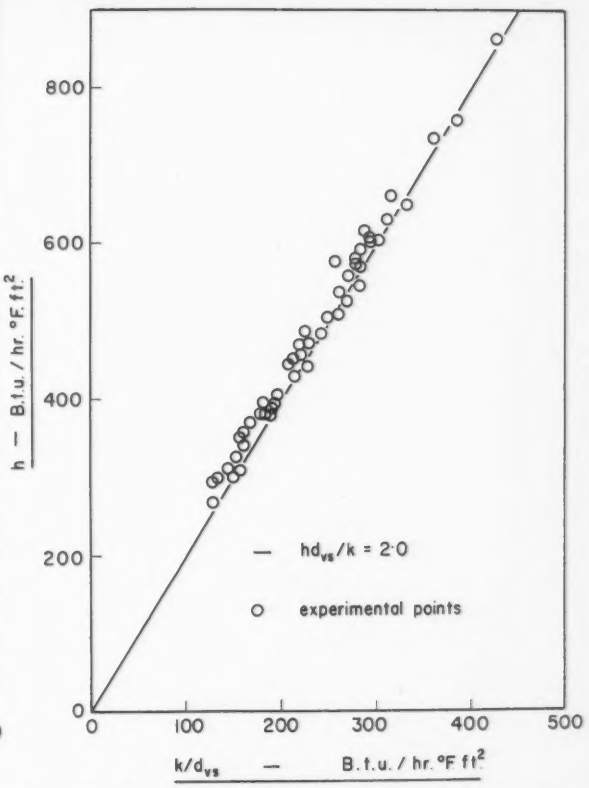

Figure 7—Comparison of experimental data with theoretical relation Nu = 2.

5. Results

A total of ten runs were made under different conditions of inlet air temperature (135.2 to 229.7°F.) air velocity (3.9 to 14.8 ft./sec.) and average droplet size (11.5 to 38.5 μ). The initial average droplet size was controlled either by changing the atomizing air pressure or by using a different nozzle. All runs were made under atmospheric pressure and no effort was made to control the inlet air humidity, which ranged from 0.0054 to 0.0123 lb. water vapor/lb. dry air.

Some of the observed values of the experimental variables as well as the calculated results are shown in Tables 1 and 2*. The calculated results include the amount of water passing any given section as calculated from the heat balance (L_{hb}) and material balance (L_{mb}), and the slope of the curves of the temperature versus distance from nozzle (dt/dx).

Three typical longitudinal temperature distributions along the spray dryer are shown in Figure 4. Figure 5 shows the fraction of water vaporized as a function of time in the spray

TABLE 1

HEAT AND MASS TRANSFER TO WATER DROPLETS OF LARGE AVERAGE DIAMETER

RUN NO. 7

Nozzle No. 22B — Atom. air pressure = 15 p.s.i.g. — Feed temp. = 95°F.

Feed rate = 6.42 lb./hr. — Drying air rate = 309 lb.d.a./hr.

Average air velocity = 3.9 ft./sec. — t_w = 95°F.

OBSERVED					CALCULATED				
x ft.	t °F.	H lb.w./lb.d.a.	d_{vs} μ	L_{hb} lb./hr.	L_{mb} lb./hr.	dt/dx °F./ft.	h B.t.u./hr.ft.²°F.	Nu —	Nu' —
0	213.6	0.0087		6.42	6.42				
0.79	168.0		38.5	3.22		−46.2	270	2.05	1.91
0.96	160.5		38.0	2.67		−36.1	243	2.21	2.04
1.13	154.7		36.9	2.33		−31.0	299	2.20	2.01
1.29	149.8		33.7	1.93		−27.0	314	2.13	1.95
1.46	145.5		32.3	1.62		−23.0	328	2.13	1.94
1.79	138.3	0.0255	30.8	1.07	1.23	−14.0	343	2.14	1.94
1.96	135.7			0.97					
2.86	130.0			0.58					

TABLE 2

HEAT AND MASS TRANSFER TO WATER DROPLETS OF SMALL AVERAGE DIAMETER

RUN NO. 10

Nozzle No. 12 | Atom. air pressure = 44 p.s.i.g. | Feed temp. = 85°F.

Feed rate = 4.86 lb./hr. | Drying air rate = 860 lb.d.a./hr.

Average air velocity = 10.7 ft./sec. | t_w = 86°F.

OBSERVED					CALCULATED				
x ft.	t °F.	H lb.w./lb.d.a.	d_{vs} μ	L_{kb} lb./hr.	L_{mb} lb./hr.	dt/dx °F./ft.	h B.t.u./hr.ft.²°F.	Nu —	Nu' —
0	161.2	0.0097		4.86	4.86				
0.96	154.0		18.3	3.35		25.7	560	2.06	1.92
1.13	150.3		17.5	2.71		21.1	571	2.03	1.88
1.29	147.1		16.9	2.11		17.3	610	2.09	1.92
1.46	144.2		15.7	1.52		13.8	660	2.09	1.94
1.79	140.5	0.0143	13.6	0.82	0.90	9.0	737	2.04	1.86
1.96	139.2		12.6	0.53		6.3	760	1.96	1.79
2.54	137.0		11.5	0.12		1.7	863	2.02	1.85
2.86	136.6			0.05					

dryer. The very striking effect of droplet size on the rate of evaporation can be seen from these curves: for instance, runs No. 8 and 9 were carried out under identical conditions, except for the initial droplet size.

Finally, the heat transfer coefficients were plotted in Figure 6 against the mean Sauter diameter, d_{vs}, while Figure 7 shows a comparison between the same experimental points and a straight line corresponding to a theoretical Nusselt Number of 2.

6. Discussion of Results

The experimental procedure followed in this investigation was planned to permit a complete analysis of the process of evaporation from water droplets suspended in a turbulent air stream. The good agreement between the heat and material balances (L_{kb} and L_{mb} in the Tables) indicate the general accuracy of the results.

The progressive evaporation of the water droplets along the drying chamber is clearly represented by the temperature distribution curves, typical examples of which are shown in Figure 4. Starting with a gentle slope in the immediate vicinity of the nozzle, the slope slowly increases to a maximum; all curves exhibit an inflection point beyond which they fall exponentially until their slope is nearly zero. A detailed study of the nozzle range has already been presented by Manning[14] and – in confirmation of his observations – the present temperature distribution data indicate that the amount of water evaporated in the first few inches from the nozzle is comparatively small. This is due to the fact that the droplets leave the nozzle at a high initial velocity, and although their rate of evaporation is high (due to their high relative velocity) their residence time in the nozzle zone is too small to permit any large amount of evaporation.

In the evaporation zone as shown by Figure 7, the average value of the Nusselt Number for all experimental points was found to be 2.07 ± 0.06. The average value of the modified Nusselt Number, Nu′, was 1.89 ± 0.06, but this somewhat lower value can be attributed to uncertainties in the estimation of the diffusivity coefficients[5].

*Tables 1 to 10 of this paper have been deposited as Document No. 6344 with the ADI Auxiliary Publications Project, Photoduplication Service, Library of Congress, Washington 25, D.C. A copy may be obtained by citing the Document No. and by remitting $1.25 for photoprints, or $1.25 for 35 mm. microfilm. Advance payment is required. Make cheques or money orders payable to: Chief, Photodupliaction Service, Library of Congress.

Conclusions

The results obtained indicate conclusively that the rate of evaporation in spray drying can safely be calculated by assuming that the individual droplets evaporate at a rate corresponding to stagnant conditions, i.e. by assuming the Nusselt Number to be equal to two, as predicted by Equation (4) for Re = 0. This is in agreement with the results of Kesler[13] who also showed that, for drops in the same diameter range as in the present study, the effective relative velocity between the droplets and the air stream was pratically zero, in spite of the air turbulence. It is furthermore apparent that the presence of the droplets in the form of a cloud has no influence on the rate of evaporation, at least at the voidage ratio commonly encountered in spray drying.

Because it accounts for the bulk of the evaporation which occurs in a spray dryer, the evaporation zone is of considerable importance in the development of a theory of spray dryer design. To calculate the residence time needed to vaporize the largest drops produced by the nozzle – which will determine the length of the evaporation zone for a given air flow – it is necessary to estimate the progressive decrease in air temperature and humidity as evaporation progresses, since the latter dictate the instantaneous rates of heat and mass transfer to the largest drops. The calculations can be readily carried out by an iterative method over small increments of time, if the drop size distribution is known. As proposed by Marshall[20], the method consists of dividing the spray into a small number of drop size groups (from six to ten, depending on the accuracy required) and of performing the calculations on each size group over a small increment of time, using the d_{vs} for that group in the correlation: $Nu = hd_{vs}/k_f = 2$.

The accuracy of the method is demonstrated by Figure 8, which compares the experimentally observed size distribution in run No. 2 at a distance 5.2-ft. from the nozzle, with that *calculated* from the experimental drop distribution measured at 3.19-ft. from the nozzle. The agreement between the two distributions is excellent.

Once the evaporation occurring in each size group over a small increment of time has been determined, it is an easy matter to calculate the resulting changes in air temperature and humidity for the interval. This in turn permits to calculate the corresponding evaporation from the largest drops produced by the atomizing nozzle.

The method of approach which has been outlined requires a knowledge of the initial drop size distribution. If the latter can be

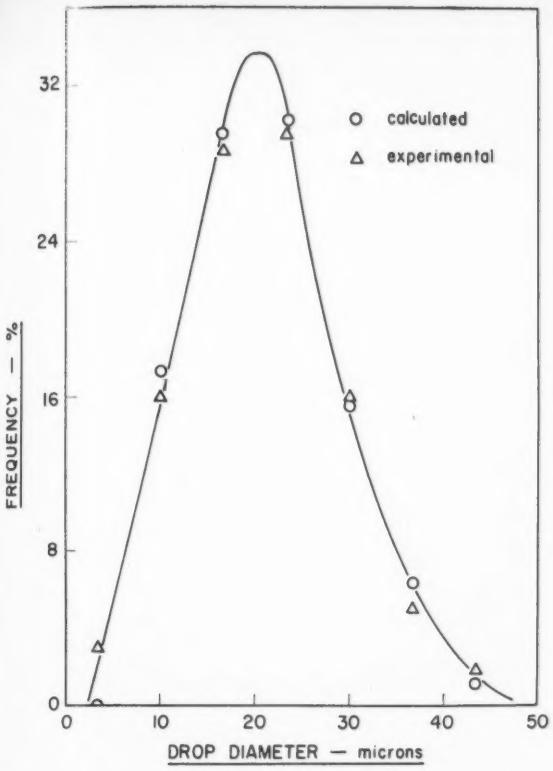

Figure 8—Calculated and experimental droplet size distribution.

expressed in the form of a simple mathematical probability function and if the vapor pressure of the solvent can be assumed to remain unaffected by the presence of a solute, the analytical method of Probert[21] can be used, and a tedious iterative solution is not necessary. (This method, however, ignores the temperature drop in the air as evaporation proceeds). A number of such distribution functions have been proposed for certain atomizing nozzles[22]. In general, however, it will be necessary to determine the distribution (and the size of the largest drop) experimentally for a given nozzle and for a specific feed liquid. The small amount of evaporation occurring in the nozzle zone can be either neglected (which will lead to a conservative estimate of the evaporation zone proper) or, preferably, the experimental data of Manning[14] and others[15,16,17] can be used. A completely analytical solution of the complex mass and heat transfer phenomena occurring in the nozzle range will only be possible when accurate data for the coefficient of drag in that region become available. Such a study is currently under way.

The present investigation has been concerned with the evaporation of clouds of water alone. The information obtained can be easily extended to more complex cases, some of which have already been studied, such as the effect of the presence of a solute in the feed solution[23] and the behavior of droplets evaporating in a centrifugal field[24]. Many more considerations still require investigation, particularly those associated with the turbulence aspects of the system, but it can now be predicted that a solution to the problem of spray dryer design on a sound theoretical basis may soon be possible.

Acknowledgements

Financial assistance from the National Research Council of Canada in the form of a research grant and of a research fellowship awarded to one of the authors, J. Dlouhy, is gratefully acknowledged. Recognition is also due to the Pulp and Paper Research Institute of Canada for the extensive use of their facilities.

Nomenclature

A = transfer area, ft.²
C_{p_f} = mean heat capacity of gas film surrounding drop, (B.t.u.)/(lb.)(°F.).
C_{p_v} = heat capacity of water vapor, (B.t.u.)/(lb.)(°F.).
c_s = humid heat capacity, (B.t.u.)/(lb.)(°F.).
D_v = diffusivity of water vapor in air, ft.²/hr.
d = individual drop diameter in a size distribution count, microns.
d_{vs} = mean drop Sauter diameter, $\Sigma nd^3/\Sigma nd^2$, ft.
g = acceleration due to gravity, ft./hr.²
h = heat transfer coefficient, (B.t.u.)/(hr.)(ft.²)(°F.).
H = air humidity, lb. water/lb. dry air.
k_f = mean thermal conductivity of the gas film surrounding drop, (B.t.u.)/(hr.)(ft.)(°F.).
k_G = mass transfer coefficient, lb. moles/(hr.)(ft.²)($\triangle p$).
L = rate of liquid spray, lb./hr.; L_{hb}, calculated from heat balance; L_{mb}, calculated from material balance.
M_m = average molecular weight of gases between the drop surface and the bulk air, lb.
m = diffusion or evaporation, lb.
n = number of droplets in a size distribution count.
p = water vapor pressure in bulk air, *p.s.f.a.*
p_f = mean pressure of air in film, *p.s.f.a.*; defined by: $p_f = \pi - (p_s - p)/2$.
p_s = equilibrium vapor pressure at the drop surface (corresponding to t_w), *p.s.f.a.*
r_o = radius of droplet, ft.
r_b = outer radius of film around droplet, ft.
s = factor $= 4\pi r_o r_b/(r_b - r_o)$, Equation (1).
S_w = specific surface area of drops, ft.²/lb.
t = temperature of air, °F.
t_w = wet bulb temperature of air, °F.
V = velocity of drying air relative to drop, ft./hr.
V_a = absolute velocity of drying air, ft./hr.
V_t = terminal velocity of drops, ft./hr.
w = air rate, lb. dry air/hr.
x = distance from nozzle, ft.
β = coefficient of volumetric expansion, $1/T$, °$R.^{-1}$.
λ_w = latent heat of evaporation at t_w, (B.t.u.)/(lb.).
μ_f = mean absolute viscosity of gas film surrounding drop, (lb.)/(ft.)(hr.).
π = atmospheric pressure, *p.s.f.a.* (in definition of p.).
ρ = density of water, (lb.)/(ft.³).
ρ_f = mean density of the gas film surrounding drop, (lb.)/(ft.³).
ρ_v = density of vapor, (lb.)/(ft.³).
θ = time, hr.
Gr = Grashof Number, $(d_{vs}^3 \rho_f^2 g/\mu_f^2)(\beta \triangle t)$.
Nu = Nusselt Number, hd_{vs}/k_f.
Nu' = Modified Nusselt Number, $k_G M_m d_{vs} p_f/D_v \rho_f = k_G d_{vs} RT/D_v$.
Pr = Prandtl Number, $C_{p_f}\mu_f/k_f$.
Re = Reynolds Number, $d_{vs} V \rho_f/\mu_f$.
Sc = Schmidt Number, $\mu_f/D_v \rho_f$.

References

(1) Morse, H. W., Proc. Am. Acad. Arts and Sci., **45**: 363 (1910).
(2) Langmuir, I., Phys. Rev., **12**: 368 (1918).
(3) Fuchs, N., Physik. 2. Sowjetunion, **6**: 224 (1934).
(4) Froessling, N., Gerlands Beitr. Geophys., **52**: 170 (1938).
(5) Ranz, W. E., and Marshall, W. R., Jr., Chem. Eng. Progr., **48**: 141, 173 (1952).
(6) Godsave, G. A. E., "Collected Papers of the 4th Int. Symp. on Combustion", Cambridge, Mass. (September 1952).
(7) Marshall, W. R., Jr., Chem. in Canada **7**: 37 (1955).
(8) Spalding, D. B., Proc. Roy. Soc. (London), A-221: 78 (1954).
(9) Ranz, W. E., Trans. Am. Soc. Mech. Eng., **78**: 909 (1956).
(10) Sleicker, C. A., Jr., and Churchill, S. W., Ind. Eng. Chem. **48**: 1819 (1956).

(11) Liu, Vi-Cheng, Dept. of U.S. Air Force, Project 2160 (1955).

(12) Soo, S. L., Chem. Eng. Sci., **5**: 57 (1956).

(13) Kesler, G. H., D. Sc. Thesis, Mass. Inst. Technol., (1952).

(14) Manning, W. P., and Gauvin, W. H., A.I.Ch.E.J. (In press).

(15) Ingebo, R. D., Nat. Adv. Comm. Aero. Tech. Note 3762 (1956).

(16) Fledderman, R. G., and Hanson, A. R., Eng. Res. Inst., University of Michigan, Report No. CM 667 (1951).

(17) York, J. L., and Stubbs, H. E., Trans. Am. Soc. Mech. Engrs., **74**: 1157 (1952).

(18) Pinder, K. L., M. Eng. Thesis, McGill University, Montreal, Quebec (1952).

(19) Rupe, J. H., "Third Symposium on Combustion Flame and Explosion Phenomena", The Williams and Wilkins Co., Baltimore (1949).

(20) Marshall, W. R., Jr., Trans. Am. Soc. Mech. Engrs., **77**: 1377 (1955).

(21) Probert, R. P., Phil. Mag., **37**: 94 (1946).

(22) Marshall, W. R., Jr., "Atomization and Spray Drying", Chemical Engineering Progress Series, No. 2, Vol. 50 (1954).

(23) Dlouhy, J. and Gauvin, W. H., A.I.Ch.E.J. **6**: 29 (March, 1960).

(24) Gauvin, W. H., Knelman, F. H., and Pinder, K. L., presented at the Symposium on Spray Mechanisms, Annual A.I.Ch.E. Meeting. Cincinnati, Ohio (Dec. 1958).

★ ★ ★

LETTERS TO THE EDITOR

A Note on Thermodynamic Consistency of Ternary Vapor-Liquid Equilibrium Data, by Li and Lu, C.J.Ch.E., 37, 117-120, 1959.

London, England

Editor, C.J.Ch.E.:

The authors have discussed a new way of applying established relationships to experimental data, and claim that it enables them to select inconsistent values from a set of vapor-liquid equilibrium data in a ternary system. This claim can be disputed in two regards. Firstly, for the three methods suggested for solving their integral Equation (5), they have only provided two examples of calculations. This is itself highly selective and particularly unwarranted if comparison is not made to other methods previously used for evaluation of the same data.

In the second place, within their calculation sets there is also unwarranted selection of data. For example, in Table 1, and Figure 1, ten experimental points from their reference 8 are considered (corresponding to runs 29, 31 - 39 of the original work). The authors then test these 10 points and show that there is an "overall deviation in thermodynamic consistency" of about 38%, which is reduced to 6% if points 29, 31 and 33 are omitted. They therefore claim that these latter 3 points are inconsistent. However, if the original 10 points *plus run 40* are examined, the deviation drops from 38% to below 14% even though it includes the so-called inconsistent points 29, 31 and 33. It seems clear then that the method advocated by the authors is neither sensitive nor critical enough to meet the claims made.

One other minor criticism may also be made. The authors claim that in the testing of isobaric data, the assumption of Broughton and Brearley (Ind. Eng. Chem. 47, 838, 1955) that T log γ is independent of temperature "seems questionable even for binary systems". The basis for their claim is Yu and Coull (Chem. Eng. Progress Symposium Series 48, No. 2, 38 (1952)). This reference discusses only 3 systems in this context, and then only from the standpoint of White's equations (Trans. A.I.Ch.E., 41, 539, 1945). Broughton and Brearley do validate their claim reasonably well for binary and ternary systems.

The authors approach may well be a promising one but extensive testing of it will be required.

L. W. Shemilt,
Department of Chemical Engineering,
University College, London.

Ottawa, Ont.

Editor, C.J.Ch.E.:

We wish to thank Dr. Shemilt for his kind interest in our publication. In reply to his criticism and comments, we would like to offer the following:

1. In our paper, the proposed graphical and numerical integration methods are developed theoretically. They are intended to illustrate the usefulness of the Gibbs-Duhem equation in its exact form. This is not the case where empirical equations are proposed, using data fitting as the only means for their justification. In the development of the proposed methods, restrictions involved in other methods are avoided, as indicated in the manuscript. To provide too many examples of calculation seems wasteful and unnecessary. The idea of extensive testing of data for supporting the Gibbs-Duhem equation is untenable and the validity of an exact method should not be judged by empirical methods simply because they are available.

It might be mentioned that our proposed methods have already been employed in the literature for testing ternary vapor-liquid equilibrium data (e.g. K. W. Free and H. P. Hutchison, J. of Chem. and Eng. Data *4*, 306 (1959)).

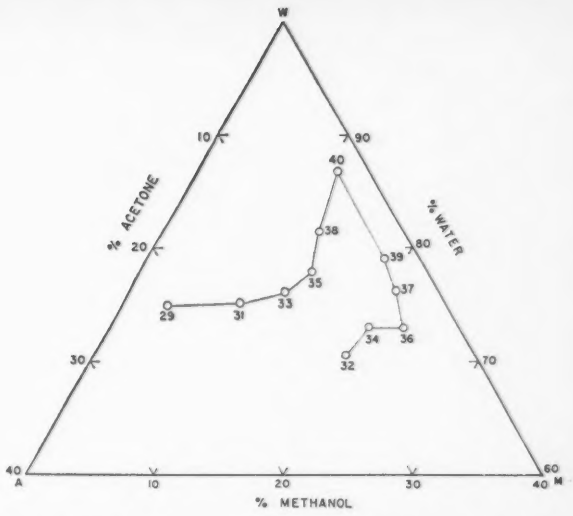

Figure 1—Arrangement of experimental points for thermodynamic consistency test.

2. We wish to point out that the calculation made in the criticism does not seem to be correct. If, from the Reference (8) of the manuscript (John Griswold and S. Y. Wong, Chem. Eng. Progress Symposium Ser. 48, No. 3, 18 (1952)), the ten points corresponding to runs 29, 31 - 39, *plus run 40* for the system acetone-methanol-water at 100°C. are examined, the logical sequence of these points should be arranged as indicated in Figure 1. It is seen in Table A that the overall deviation in the thermodynamic consistency of these eleven points is 32.3%. If the calculation is repeated, excluding points 29, 31 and 33, the deviation is reduced to 2.4%. The same conclusion is reached as that presented in the manuscript. It is unfortunate that the criticism is misleading. We have not included point 40 in our paper because it is a little too far away from a set of closely spaced points, as required in the numerical method. It should be mentioned, however, that we do not claim that there should be no possibility of mutual cancellation of positive and negative errors. Should the percentage deviation of a series of points be changed very considerably by including or excluding a single point, it would be obvious that this point is thermodynamically inconsistent.

3. In the article, it is mentioned that the validity of the assumption, $T \log \gamma_i$ (or $T \ln \gamma_i$) at constant composition is independent of temperature, is questionable. We still believe this and share the point of view of Smith and Bennett (Ind. Eng. Chem. *48*, 679-80, (1956)) regarding the Broughton and Brearley method (Ind. Eng. Chem. *47*, 838, (1955)).

The temperature dependence of $T \ln \gamma_i$ is exactly given by

$$\frac{\partial (T \ln \gamma_i)}{\partial T} = \ln \gamma_i - \frac{L_i}{RT}$$

where L_i is the partial molal heat of solution of component i. The assumption that $T \ln \gamma_i$ at constant composition is independent of temperature, as employed by Broughton and Brearley, indicates constant partial molal heat of solution, which is obviously not necessarily true. Furthermore, it requires ideal entropy of mixing for all solutions. This is shown in the following expressions:

$$\frac{\partial G^E}{\partial n_i} = RT \ln \gamma_i$$

TABLE A

Acetone-Methanol-Water at 100°C.
(John Griswold and S. Y. Wong, Chem. Eng. Progress Symposium Ser. 48, No. 3, 18 (1952))

Run. No.	x_1	$\log \gamma_1$	$x_1 (\log \gamma_{1b} - \log \gamma_{1f})$	x_2	$\log \gamma_2$	$x_2 (\log \gamma_{2b} - \log \gamma_{2f})$	x_3	$\log \gamma_3$	$x_3 (\log \gamma_{3b} - \log \gamma_{3f})$
29	0.215	0.4082	−0.01406	0.033	0.0398	+0.00316	0.752	0.0792	−0.00136
31	0.158	0.4736	−0.01506	0.088	−0.0560	+0.00200	0.754	0.0810	+0.00054
33	0.119	0.5035	−0.01297	0.119	0.0170	−0.00536	0.762	0.0785	−0.00137
35	0.089	0.5826	−0.01064	0.131	−0.0110	−0.00665	0.780	0.0828	+0.01533
38	0.066	0.6230	−0.01155	0.119	0.0678	−0.02111	0.815	0.0588	+0.03994
40	0.024	0.7576	−0.00006	0.107	0.1664	−0.00728	0.869	0.0338	+0.01790
39	0.028	0.6255	+0.00465	0.182	0.1358	+0.00906	0.790	0.0382	−0.00442
37	0.033	0.5917	+0.00378	0.204	0.1166	+0.00590	0.763	0.0394	−0.02258
36	0.043	0.5110	+0.00336	0.225	0.1069	+0.01140	0.732	0.0678	−0.02938
34	0.069	0.5136	+0.00128	0.198	0.0660	+0.01486	0.733	0.0795	−0.02082
32	0.100	0.4925	+0.00211	0.193	0.0318	+0.00659	0.707	0.0962	−0.01179

$\Sigma + = +0.14186$
$\Sigma - = -0.19646$
Total = −0.05460
% Deviation = 32.3%

Repeat the above calculation without run nos. 29, 31 and 33

$\Sigma + = +0.13953$
$\Sigma - = -0.14291$
Total = −0.00338
% Deviation = 2.4%

$$\frac{\partial (RT \ln \gamma_i)}{\partial T} = \frac{\partial^2 G^E}{\partial n_i \cdot \partial T} = \frac{\partial S^E}{\partial n_i} = S_i^E = 0$$

where G^E and S^E are the excess free energy and entropy of mixing, respectively. Such solutions having ideal entropy of mixing are classified as "regular" solutions. The invalidity of the assumption that all solutions behave as regular solutions is beyond argument. For detailed discussion, see for example, "Chemical Thermodynamics" by Prigogine and Defay, translated by Everett, Chapters XXIV and XXV, Longmans Green and Co. London, (1954).

In 1956, Smith and Bennett (Ind. Eng. Chem. *48*, p. 680, Column I, lines 32-4, (1956)) in their review article on thermodynamics pointed out that "The assumption that $T \log \gamma$ is constant at constant composition is only roughly true in a few cases and is often incorrect." Recently, Lu (Can. J. Chem. Eng. *37*, 193, (1959)) correlated some heats of mixing data available in the literature and reported that they vary linearly with temperature for many systems over a moderate temperature range. In other words, the quantity $\log \gamma$. at constant composition should involve three terms, of the form $a + (b/T) + c \log T$. In addition to the paper by Yu and Coull (Chem. Eng. Progress Symposium Series *48*, No. 2, 38 (1952)), one may cite many other evidences to show that the assumption, that $T \log \gamma_i$ at constant composition is independent of temperature, is indeed questionable.

James C. M. Li,
Monroeville, Pa., U.S.A.
and
Benjamin C.-Y. Lu,
Chemical Engineering Department,
University of Ottawa.

★ ★ ★

Effect of Diesel Locomotive Operation on Atmospheric Conditions in a Railway Tunnel[1]

R. P. RENNIE[2], *Z. JEGIER*[2] *and MORRIS KATZ*[3]

An extensive study was made over a seven day period to determine if it would be feasible, from an air pollution view point, to operate diesel locomotive powered trains through the St. Clair Tunnel. The test involved the passage of approximately 200 diesel powered freight and passenger trains through the tunnel; 3,000 air samples were taken and measurements were made on air flow and smoke density. Concentrations of carbon monoxide, nitrogen dioxide, total oxides of nitrogen, aldehydes, sulphur dioxide, carbon dioxide and oxygen were determined.

The sampling methods, sampling equipment, analytical procedures and test equipment used for this particular investigation should be applicable to a variety of air pollution problems met in the chemical industry.

The arrival of the era of the diesel locomotive on the Canadian National Railways made confirmation necessary that diesel exhaust fumes in low concentrations were not detrimental to atmospheric conditions in various installations.

One of the early developments of the change to diesel power required this confirmation in the case of the replacement of electrified by dieselized trains in the Sarnia Tunnel, which forms a major international traffic link betweenSa rnia, Ontario and Port Huron, Michigan.

This paper, therefore, presents the engineering and chemical results of tests carried out in this tunnel under fully dieselized operation in October 1957 and October 1958 and deals with the techniques of approaching and analyzing the factors involved in the investigation. The toxicological aspects of the work have been presented in a paper at the Industrial Health Conference of the American Industrial Hygiene Association[1].

Similar tests have been carried out on other railroads[2], but as far as is known, the present work represents one of the most intensive studies of a railway tunnel environment under conditions of fully dieselized operation which has been carried out to date. For the purposes of the tests, it was necessary to suspend all electrically hauled traffic and replace it by diesel powered trains for a period of seven days. Chemical, engineering and medical staffs were involved in the investigation.

The test data obtained confirmed that exhaust fumes resulting from full dieselization of the traffic through the tunnel were not significantly detrimental to atmospheric conditions in the tunnel. The mean concentrations of constituents of exhaust gases were, in general, below the threshold limits established by the American Conference of Governmental Industrial Hygienists. There were no abnormal health conditions observed on participants during 8 hr. exposure to the tunnel atmosphere.

In order to reduce concentrations of smoke and total oxides of nitrogen to well below acceptable levels and to provide a margin of safety in the event of unusual operation conditions, it was recommended that a system of forced ventilation be installed before full dieselization was introduced as standard operating practice to replace electrical operation of trains.

Diesel Engine Exhaust

Diesel exhaust fumes contain certain gases resulting from the complete or partial combustion of diesel fuel oil and also formed during combustion with the excess air supplied in engine operation[3,4]. The more harmful components of the exhaust gases are carbon monoxide, carbon dioxide, oxides of nitrogen, oxides of sulphur, formaldehyde and smoke[5]. The concentrations at which these constituents occur in diesel exhaust largely depend on the fuel/air ratio which in turn varies with the load on the engine[6].

The trials in the St. Clair Tunnel were conducted using 1750 Class GR-17 road switchers of General Motors manufacture. In these engines the air blower, providing air for combustion, is driven directly off the drive shaft and therefore air intake is proportional to engine speed. Figure 1 shows the volumes of combustion air, exhaust gases and excess air at various engine speeds for units of this type.

At a given speed, the weight of air intake per unit time is approximately constant, whereas the weight of fuel injected increases as the load on the engine increases. Under normal working conditions the excess of air used may be much greater than the stoichiometric requirement.

A study carried out in 1946 by Berger and McGuire, reported findings on diesel exhaust gas composition[7]. The locomotive investigated developed 1570 h.p., at maximum speed, from each of its four units. Apart from these results, there has been little published information on the exhaust of high horsepower locomotive engines such as those used throughout these tests. The Canadian National Railways Research Laboratories, however are conducting investigations in this field, the results of which will be reported at a future date. Preliminary results indicate that the range of constituent gas concentrations in the exhaust gas of newly reconditioned engines 1750 h.p., is as shown in Table 1.

The St. Clair Tunnel

The St. Clair Tunnel has a length of 6,032 ft. and at its midpoint lies 25 ft. beneath the bed of the St. Clair River. (Figure 2) The tunnel is of tubular shape consisting of a cast iron shell approximately 20 ft. in diameter and having a cross-sectional area of 312 sq. ft. and a volume of 1,875,000 cu. ft. (Figure 3) It has a single track and the slope of the approach

[1]*Manuscript received September 10, 1959; accepted February 12, 1960.*
[2]*Department of Research and Development, Canadian National Railways, Montreal, Que.*
[3]*Department of National Health and Welfare, Ottawa, Ont.*

TABLE 1
CONCENTRATIONS OF SOME EXHAUST CONSTITUENTS FROM NEWLY RECONDITIONED 1,750 H.P. DIESEL LOCOMOTIVES

Exhaust Constituent	Concentration in p.p.m.		
	Idling	Half Load Notch 4	Full Load Notch 8
Carbon monoxide	80 – 110	60 – 105	475 – 480
Nitrogen dioxide	65 – 70	250 – 305	330 – 490
Total oxides of nitrogen	80 – 90	355 – 410	440 – 920
Formaldehyde	3 – 7	2 – 3	4 – 10

and outbound grades is 2%. Because of the unique elevations in the tunnel and the cooling effect of the river and the mass of soil above the tunnel, it was anticipated that there would be little, if any, natural ventilation. Nevertheless, in view of the operational train speed of 15 m.p.h. and the fact that the frontal area of a diesel or car unit is approximately one-half that of the cross-sectional area of the tunnel, a piston action by the train could be expected to draw a certain quantity of diluting air into the tunnel with beneficial effect[8].

Methods of Sampling and Analysis

The shape, dimensions and the absence of forced ventilation in the tunnel suggested the possibility of variations in exhaust gas concentrations at different points along the length of the tunnel. In addition, trains enter the tunnel on a down grade under their own momentum with engines idling and coast to about the mid-point; here power is gradually applied until the locomotive engines are at full power at the outbound grade. In order to contend with this situation, it was necessary to collect air samples representing not only average conditions, but also fluctuating, peak and residual conditions.

Sample collecting stations were therefore chosen at points 600 ft. inside the tunnel portals and at the mid-point of the tunnel to insure that the samples collected would be representative of tunnel conditions. A diagram showing the locations of the various test stations is shown in Figure 2.

Personnel engaged in the work of air sampling were employed on an 8 hr. 3-shift basis. In all, 218 trains passed through the tunnel from both easterly and westerly directions during the test. Trains were powered with from one to four diesel units and speeds were varied between 12 and 25 m.p.h. Special idling tests inside the tunnel were conducted using two unit diesel locomotives.

"Average" air samples were collected in automatic absorption samplers in which a measured volume of air controlled by a calibrated orifice passed through the absorption solution for 10 minutes. Average samples were collected for nitrogen dioxide, carbon dioxide, sulphur dioxide and aldehydes.

"Instantaneous" air samples were collected by breaking the seals of calibrated one-litre glass tubes that had been evacuated to a pressure of less than 1 mm. of mercury. Instantaneous samples were collected for carbon monoxide, nitrogen dioxide, total oxides of nitrogen, aldehydes and oxygen. The glass inlet seals were snapped off at the following specified times:

1. Summit — Train leaving yard
2. Zero time — Train passing sampling station
3. Zero + 3 minutes
4. Zero + 6 minutes

Continuous sampling for smoke and particulate matter was carried out by A.I.S.I. Hemeon Samplers and by High Volume Samplers respectively[9,10].

Special sampling for blood tests on personnel at the three gas sampling stations in the tunnel before and after each 8 hr. exposure was conducted by Medical Staff of the Department of National Health & Welfare and the Canadian National Railway Company. These blood samples were subsequently analyzed for carboxyhaemoglobin content.

Air flow measurements, temperature, relative humidity and barometric pressure observations were made during and after the passage of each test train.

Methods of analysis were chosen, taking into account factors such as possible comparatively high or very low occurrences of gas concentrations, as well as the facilities which would be available in the temporary laboratory at Sarnia. Consideration was also given to the effects of storage and transportation on samples which might have to be sent some 400 miles to the company's main laboratories, for final analysis.

Nitrogen dioxide and aldehydes were determined as soon as possible (approximately 2 hrs.) after collection of the samples.

Nitrogen dioxide concentrations were determined by the Saltzman colorimetric procedure. This method depends on the reaction of nitrogen dioxide, sulphanilic acid and N-(1-naphthyl)-ethylenediamine in acetic acid[11]. Sensitivity of the method is about 0.05 p.p.m.

Aldehydes were absorbed in an aqueous solution of phenylhydrazine hydrochloride followed by treatment with potassium ferricyanide in alkaline solution[12,13]. The sensitivity of this procedure is approximately 0.2 p.p.m.

Sulphur dioxide was absorbed in a dilute solution of sulphuric acid and hydrogen peroxide[14,15]. Specific conductance of the resultant sulphuric acid was measured by a conductivity bridge. The particular instrument used was supplied by the Industrial

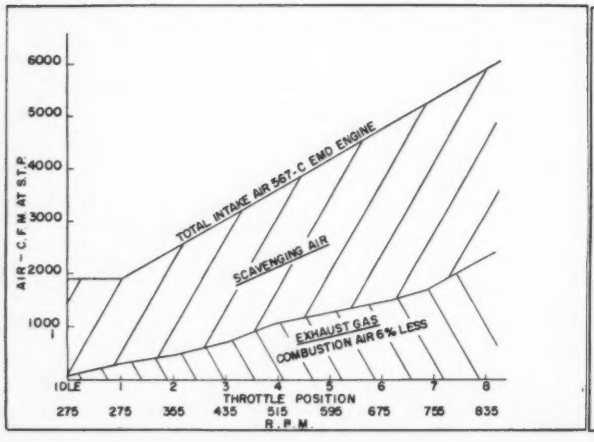

Figure 1—Intake air and exhaust. 1750 h.p.-G.M. engine.

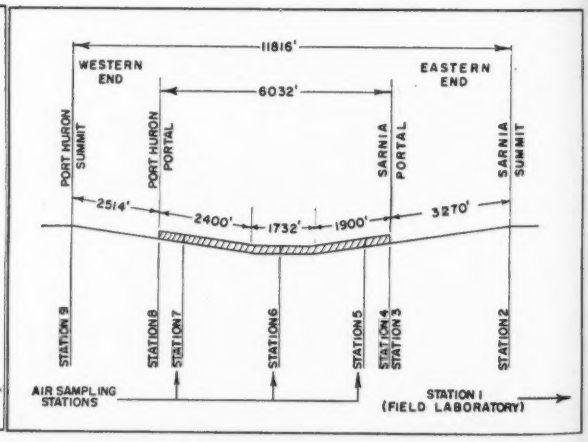

Figure 2—Longitudinal section of St. Clair tunnel and location of air sampling stations.

Instrument Company, and was designated Model RC-1. The cell constant of the conductivity cell was 0.1 mhos. A sensitivity of about 0.05 p.p.m. was obtained in these determinations by the specific method employed.

Carbon dioxide was absorbed in barium hydroxide containing barium chloride[16]. The concentration was estimated from the amount of neutralized barium hydroxide. The sensitivity of this method is approximately 25 p.p.m.

Total oxides of nitrogen at the time of the investigation were determined by the modified phenoldisulphonic acid method prepared by the Research Department of the Union Oil Company of California as a tentative method to A.S.T.M. Committee D-22[17]. Total oxides of nitrogen were calculated as NO_2. This method has a sensitivity of approximately 5 p.p.m.

Carbon monoxide in instantaneous samples was determined by passing the air sample through the NBS colorimetric indicating gel[18,19]. This gel contains ammonium molybdate and palladium sulphate. The color produced was compared with standards prepared in a similar manner from air containing 0.074% CO. This method has a sensitivity of approximately 0.2 p.p.m. Carbon monoxide concentrations were also recorded continuously by the M.S.A. direct indicating instrument[20]. The working principle of this instrument is based on the measurement of the heat of oxidation reaction of carbon monoxide to carbon dioxide over the catalyst "Hopcalite". The sensitivity of this instrument is approximately 0.002%.

Carbon monoxide in the blood of personnel was determined by means of the microgasometric technique of Scholander and Roughlan[21]. Some samples were analyzed by the infra-red absorption technique[22].

Smoke concentrations were determined by filtration of a measured volume of air through paper tape in A.I.S.I. (Hemeon) smoke samplers and evaluation of the spot by optical transmittance. Smoke was sampled continuously on an hourly cycle and the concentrations were calculated in COH units per 1,000 linear feet of air filtered. Particulate matter was determined by filtration over 8 hr. periods through 1,106 flash-fired Fiberglas web in high volume samplers, followed by gravimetric determination of the Fiberglas deposits. The results are expressed as milligrams per cubic meter of air.

Air flow measurements were obtained by means of calibrated velometers and annemometers.

Discussion of Test Results

The maximum allowable concentrations of each toxic gas and irritant in the atmosphere for continuous exposure during an 8 hr. period have been established by a Committee of the American Conference of Governmental Industrial Hygienists. The threshold values are revised each year in the light of the most up-to-date information and experimentally verified data on toxicity[23].

The 1958 revision shows the following maximum allowable concentrations (M.A.C.):

Carbon dioxide	5,000 p.p.m.
Carbon monoxide	100 p.p.m.
Total oxides of nitrogen	25 p.p.m.
Nitrogen dioxide	5 p.p.m.

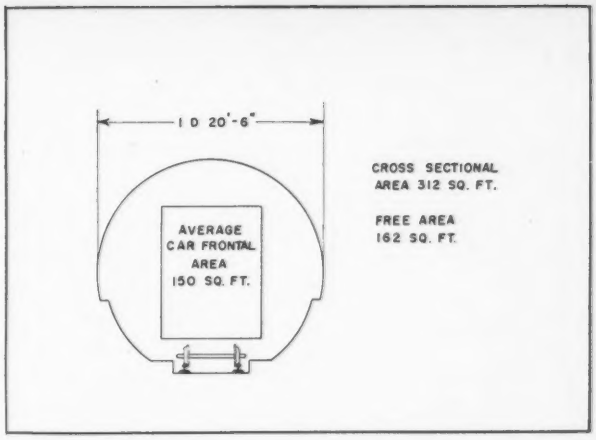

Figure 3—Cross section of St. Clair tunnel.

Sulphur dioxide	5 p.p.m.
Formaldehyde	5 p.p.m.

Typical concentrations of the gases found in the tunnel atmosphere during the passage of diesel trains are presented:

(a) *Carbon Monoxide*

Concentrations of carbon monoxide found in the tunnel were well within safe limits. With only 2 exceptions, one of which can be noted in Table 2 at 150 p.p.m., concentrations were well below the M.A.C. of 100 p.p.m. for an 8 hr. exposure period. Table 2 gives a summation of results at the gas sampling station in the middle of the tunnel.

Carboxyhaemoglobin contents in the blood of test personnel after 8 hrs. exposure to the tunnel environment, are shown in Table 3. The pre-exposure percentages roughly parallel individual smoking habits[24,25]. Post-exposure figures indicate a slight trend toward higher HbCO saturation percentages in approximately half of the subjects. This is in substantial agreement with the fluctuating, but generally low, carbon monoxide concentrations found in the tunnel atmosphere. (Table 3)

(b) *Aldehydes*

As indicated in Table 4 showing results for aldehydes at the sampling station in the centre of the tunnel, concentrations of aldehydes were generally below the M.A.C. of 5.0 p.p.m.

(c) *Oxides of Nitrogen*

Typical values for oxides of nitrogen are shown in Table 5 at the gas sampling station nearest the Port Huron portal.

Average values for all samples taken for nitrogen dioxide were well below the M.A.C. of 5 p.p.m.

Total oxides of nitrogen expressed as nitrogen dioxide found in approximately 190 samples collected during the passage of test trains showed concentrations considerably in excess of 25 p.p.m. This value, although not recognized by A.C.G.I.H.,

TABLE 2
CARBON MONOXIDE CONCENTRATIONS IN P.P.M. IN ST. CLAIR TUNNEL AT STATION 6 (MIDDLE)

Date	Time	No. of Samples	Mean	Highest Concentration	% values exceeding M.A.C. of 100 p.p.m.
Oct. 22	12 a.m. – 8 a.m.	17	3.5	10	0
	8 a.m. – 4 p.m.	18	3.8	20	0
	4 p.m. – 12 p.m.	15	2.7	15	0
Oct. 23	12 a.m. – 8 a.m.	14	2.8	10	0
	8 a.m. – 4 p.m.	7	2.4	8	0
	4 p.m. – 12 p.m.	14	13.6	150	7

TABLE 3
CARBON MONOXIDE AS PER CENT SATURATION OF CARBOXYHAEMOGLOBIN IN BLOOD OF PERSONNEL EXPOSED TO TUNNEL ATMOSPHERE FOR 8 HOURS

Subject	Exposure Time	HbCO Saturation %		Smoking Habit
		Before	After	
A	12:01 a.m.– 8:00 a.m.	7.50	10.60	Light
B	,, ,,	3.14	2.84	Moderate
C	,, ,,	8.50	9.35	Heavy
D	,, ,,	4.23	4.0	Nil
E	,, ,,	6.40	8.0	Moderate
G	8:00 a.m.– 4:00 p.m.	7.10	8.0	Nil
H	,, ,,	2.25	2.4	Moderate
J	,, ,,	5.32	6.63	Light
K	,, ,,	4.17	6.85	Moderate
L	,, ,,	4.12	8.85	Moderate
M	4:00 p.m.–12:00 p.m.	7.15	9.30	Moderate
O	,, ,,	6.73	6.82	Heavy
P	,, ,,	2.21	2.27	Nil
S	,, ,,	2.67	9.60	Light

nevertheless serves as a guide to a possible threshold value, since it has been established that values below 25 p.p.m. are not of significant hazard. The average of all samples taken was approximately 26 p.p.m. with mean values at the sampling stations varying from 9.1 to 38.4 p.p.m. and the peak instantaneous concentration reaching a level of 67 p.p.m.

This substantial difference between concentrations of nitrogen dioxide and total oxides of nitrogen results from the presence of nitric oxide in diesel exhaust gas. At the high combustion temperatures existing in diesel engines, the reaction $N_2 + O_2 = 2NO$ takes place. This reaction has been mentioned by Davis and Holtz. Temperature and oxygen concentrations result in oxides of nitrogen varying from NO to mixtures of NO and NO_2.

Apart from this, a number of reactions occur where mixtures of nitrogen dioxide, nitric oxide, oxygen and water vapor are present in the diesel exhaust[26,27]. These result in the conversion of nitric oxide to nitrogen dioxide or nitrous acid:

$$2NO + O_2 = 2NO_2$$
$$NO + NO_2 + H_2O = 2HNO_2$$

In the equilibrium condition, where the concentrations of nitric oxide and nitrogen dioxide are equal and about 2% water vapor is present, the product (nitrous acid) would be about 19% of the nitric oxide concentration.

The rate law governs the conversion of the nitric oxide and oxygen to nitrogen dioxide[28]:

$$-\frac{d[NO]}{dt} = k[NO]^2[O_2]$$

The time required for conversion of half the nitric oxide may be calculated from the equation

$$t_{0.5} = \frac{1}{k[O_2][NO]_{\text{initial}}},$$

since the oxygen concentration in the tunnel was found to be essentially constant.

The concentrations of total oxides of nitrogen in relation to nitrogen dioxide found in the tunnel atmosphere reflect the relatively slow rate of oxidation of nitric oxide to nitrogen dioxide. This result was anticipated, since the primary oxidation product of the atmospheric nitrogen supplied for combustion with the diesel fuel oil is nitric oxide. Hence, it was expected that nitric oxide concentration in the tunnel would tend to greatly exceed those of nitrogen dioxide. Table 5 shows typical concentration levels, from which is clear that several hours would be required for conversion of appreciable quantities of nitric oxide to the much more toxic nitrogen dioxide.

Under normal operation, most of the gases are swept out of the tunnel by the ventilation caused by the piston effect of passing trains and in view of the low concentrations of nitrogen dioxide, it was considered that concentrations of oxides of nitrogen presented no serious hazard.

(d) *Smoke and Particulate Matter*

Smoke and particulate matter occurred in relatively high concentrations in the tunnel environment, especially during periods of heavy train activity. Smoke concentrations determined on an hourly basis, attained values considerably higher

TABLE 4
ALDEHYDES AS FORMALDEHYDES IN P.P.M. IN ST. CLAIR TUNNEL AT STATION 6 (MIDDLE)

Date	Time	No. of Samples	Mean	Highest Concentration	% values exceeding M.A.C. of 5 p.p.m.
Oct. 22	12 a.m. – 8 a.m.	8	1.9	3.5	0
	8 a.m. – 4 p.m.	8	3.2	4.3	0
	4 p.m. – 12 p.m.	8	2.8	3.7	0
Oct. 23	12 a.m. – 8 a.m.	8	2.7	3.9	0
	8 a.m. – 4 p.m.	3	1.5	1.5	0
	4 p.m. – 12 p.m.	6	1.4	2.0	0

TABLE 5
TOTAL OXIDES OF NITROGEN AND NITROGEN DIOXIDE IN P.P.M. AT STATION 7 (WEST) ON OCTOBER 22, 1959

Exhaust Constituent	Time	Mean	Highest Concentration	% Values Exceeding M.A.C.	M.A.C.
Total Oxides of Nitrogen as NO_2	12 a.m. – 8 a.m.	28	38	60	
	8 a.m. – 4 p.m.	17	23	0	25
	4 p.m. – 12 p.m.	28	64	50	
Nitrogen Dioxide	12 a.m. – 8 a.m.	2.5	13	12	
	8 a.m. – 4 p.m.	1.2	3	0	5
	4 p.m. – 12 p.m.	3.6	15	17	

than those usually encountered in both urban and industrial atmospheres[29,30]. The mean hourly smoke concentrations for 24 hr. periods varied from 5.3 to 10.1 COH units per 1,000 linear ft. of air, with a maximum hourly concentration of 22.4 COH/1,000 linear ft. One COH unit is defined as that quantity of light scattering solids producing an optical density of 0.01 when measured by light transmission. Parallel observations at a sampling station outside the tunnel, Station 1, yielded values of 0.4 to 3.0 COH/1,000 linear ft. whereas at Station 5 inside the tunnel the values ranged from 2.2 to 15 COH/1,000 linear ft. (Figure 4)

A variation in concentration (over 8 hr. test periods) from 0.9 to 2.3 mg./cu. m. was found for the particulate matter collected by the high volume filtration samplers. Typical values for particulate matter collected during 2 of the test days are shown in Table 6.

Smoke and particulate matter represent non-specific air pollutants that are objectional above certain minimum levels depending upon effects on visibility and possible respiratory effects. The relatively high values obtained for smoke and particulate matter were factors considered in the subsequent decision to install forced ventilation in the tunnel.

(e) *Air Flow in the Tunnel*

The displacement of part of the tunnel atmosphere by moving trains results in a piston action which pushes a considerable volume of air ahead of the train while a corresponding suction effect draws fresh air into the tunnel at the inbound portal. Smoke and exhaust gases in the form of a trailing wake or "slug" are drawn along with the train. (Figure 5)

Measured average air displacement per train was 1.54×10^6 cu. ft., which is somewhat less than the calculated volume of the tunnel of 1.87×10^6 cu. ft. Therefore, since, on the average, less than one complete air change occurred in the tunnel as a result of the passage of a train, low residual concentrations of exhaust components were found in the tunnel atmosphere. These were determined from the "Summit" samples, that is samples collected prior to entrance of trains into the tunnel. The residual levels of toxic gases in the tunnel may be also computed by means of the formula[31]:

$$C = C_o e^{-bt}$$

when C is the residual gas concentration, C_o is the original gas concentration, b is the coefficient of ventilation and t is the persistence time. The number of air displacements necessary to reduce exhaust gas concentration from C_o to C is given by bt.

For example, where an initial concentration of total oxides of nitrogen was 47.2 p.p.m. at the tunnel's midpoint, and maximum air displacement was 2.6×10^6 cu. ft., calculation of residual concentration after fresh air was drawn in by a train's passage showed the residual concentration to be 11.9 p.p.m. Where air displacement was minimal, namely 1.0×10^6 cu. ft., total oxides of nitrogen were recorded at a concentration of 25.2 p.p.m. Calculation reduces this to a residual level concentration of 14.8 p.p.m.

TABLE 6
CONCENTRATIONS OF PARTICULATE MATTER IN MILLIGRAMS PER CUBIC METRE CALCULATED FROM HIGH VOLUME FILTER WEIGHINGS

Date	Shift	Station 5	Station 6	Station 7
Oct. 22	1	1.5	1.2	1.7
	2	2.0	1.6	2.3
	3	1.7	1.1	1.5
Oct. 23	1	2.2	1.3	1.6
	2	1.5	1.2	1.0
	3	2.0	.9	1.1

Ventilation of the Tunnel

Four axial flow fans were installed, two at each portal as shown in Figure 6, with one fan on each side of the portal.

Each of these fans has an output of 57,000 c.f.m. against free air of 47,000 c.f.m. against a resistance of 2 in. of water. When the fans are reversed they can withdraw 60% of these quantities. Each fan is powered by a 20 h.p., 1,800 r.p.m., 60 cycle, 3 phase 550 v. motor. The motor is of the totally enclosed type directly coupled to the fan within the fan housing.

The fans are 50 in. in diameter on the outside of the housing. Each fan outlet is extended into the tunnel approximately 50 ft. by means of an air duct, of approximately 18 sq. ft. cross-sectional area. The fans are located just outside the portals and the ducts are fastened to the tunnel walls to maintain full established clearances for the passage of locomotives and trains.

The operation of the fans is controlled by photocells located a few feet outside each portal. The passage of a train starts all fans blowing air through the tunnel in the direction of train movement. A time delay relay permits the fans to continue operating for a pre-set interval after the train has cleared the outbound portal. This interval is adjusted from 10 to 15 minutes and is limited only by the practical interval of dispatching the next train through the tunnel. Operation of the ventilation system is supervised by remote indication and control in the

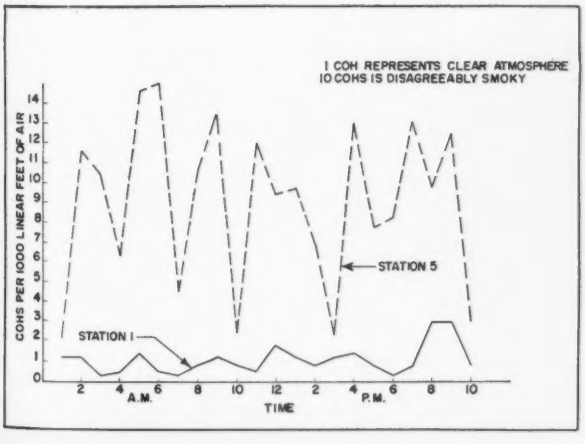

Figure 4—Hourly smoke concentrations at Stations 1 and 5 on October 23, 1957.

Figure 5—St. Clair tunnel—smoke in the form of "Slug" is drawn along with the train.

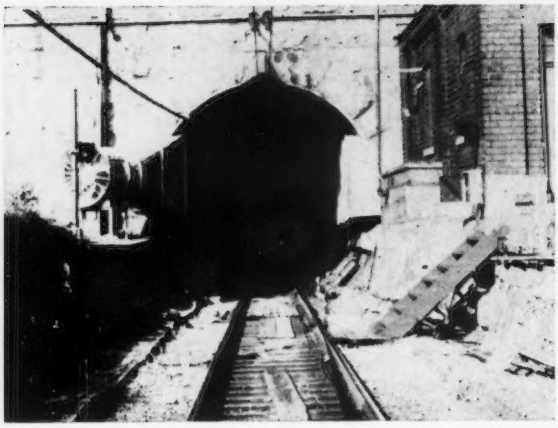

Figure 6—Ventilating fan. There are two axial flow fans installed at each portal.

dispatchers' tower at the Sarnia tunnel summit, and malfunction of the system can therefore be detected immediately.

The ventilating system induces an air velocity of approximately 3.5 m.p.h. in the tunnel and is designed to supplement the ventilation produced by the piston action of trains. This system is somewhat novel as compared to the high velocity ventilation which has been installed in several railroad tunnels. Employment of this type of system was possible due to the peculiar shape and construction of the tunnel, as described previously, which results in a considerable amount of ventilation induced by train movement and the absence of natural air flow in the tunnel as a result of variable winds and other weather conditions.

The combined capacity of the four fans that provide ventilating air to the tunnel is equal to a sufficient volume of air permitting a complete change of air in the tunnel every 10 minutes, this ventilating effect being in addition to that induced by train passage.

Extensive tests conducted in the tunnel subsequent to the installation of the ventilating system have shown that concentrations of smoke and oxides of nitrogen are reduced by approximately 30% with a corresponding reduction in concentrations of the other constituents of diesel exhaust gas.

These reductions are sufficient to bring the concentrations of all components of the exhaust fumes to well below acceptable levels and to provide an adequate safety margin for all conditions of operations.

Following the installation of the forced ventilating system and tests to evaluate its performance, full dieselized operation of the tunnel was authorized in the fall of 1958.

References

(1) Katz, M., Rennie, R. P., Jegier, Z., A.M.A. Arch. Ind. Health, **20,** No. 6 (December 1959).

(2) Ash, J. H., Naus, L. L., "Use of Diesel Engines in Tunnels", U.S. Bureau of Mines Information Circular, 7222 (October 1942).

(3) Elliot, M. A., Davis, R. F., and Friedal, R. A., "Products of Combustion from Diesel Fuel", Proceedings Third World Petroleum Congress, The Hague. Section VII, pp. 280-297 (1951).

(4) Holtz, J. C., Berger, L. B., Elliot, M. A., and Schrenk, H. H., Diesel Engines Underground, I. "Composition of Exhaust Gas from Engines in Proper Mechanical Condition", U.S. Bureau of Mines Report of Investigation, 3508 (1940).

(5) Davis, R. F., and Holtz, J. C., "Exhaust Gases from Diesel Engines", Chapter 9, pp. 74-94, of Problems and Control of Air Pollution, F. S. Malette, Reinhold Pub. Corp., New York (1955).

(6) Elliot, M. A., and Martin, A., Review of Bureau of Mines Work on Use of Diesel Engines Underground, U.S. Bureau of Mines Report of Investigations, 4381 (1948).

(7) Berger, L. B., and McGuire, L. H., "Observations on the Use of a Diesel Freight Locomotive through a Railway Tunnel", U.S. Bureau of Mines Report of Investigations, 3887 (1946).

(8) Daugherty, R. L., A.S.M.E. Trans., p. 77 (February 1942).

(9) Hemeon, W. C. L., Haines, Jr., G. F., and Ide, H. M., Air Repair, **3,** 1 (1953).

(10) Chambers, L. A., Am. Ind. Hyg. Assoc. Quart., **15,** 290 (1954).

(11) Saltzman, B. E., Anal. Chem., **26,** 1949 (1954).

(12) Kersey, R. W., Maddock, J. R., and Johnson, T. E., Analyst, **65,** 203 (1940).

(13) Tanenbaum, M., and Bricker, C. E., Anal. Chem., **23,** 354 (1951).

(14) Thomas, M. D., and Abersold, J. N., Ind. Eng. Chem., Anal. Ed., **1,** 14 (1929).

(15) Thomas, M. D., Ind. Eng. Chem., Anal. Ed., **4,** 253 (1932).

(16) Scott, W. W., "Standard Methods of Chemical Analysis", Nostrand Co., Inc., New York (1945).

(17) "Determination of Oxides of Nitrogen in Gaseous Combustion Products", Union Oil Company of California, Research Department, March (1957).

(18) Shepherd, M., Schumann, S., and Kilday, M. V., Anal. Chem., **27,** 380 (1955).

(19) Shepherd, M., Anal. Chem., **19,** 77 (1947).

(20) Katz, J. H., Reynolds, D. A., Frevert, H. W., and Bloomfield, J. J., U.S. Bureau of Mines, Technical Paper, 355 (1926).

(21) Scholander, P. F., and Roughton, F. J. W., J. Bio. Chem., **148,** 541 (1943).

(22) Bates, D. V., Clin. Sci., **11,** 21 (1952).

(23) Threshold Values for 1958, A.M.A. Arch. Ind. Health, **18,** No. 2, 178 (August 1958).

(24) Minchin, L. T., Coke and Gas, **16,** 425 (1954).

(25) Parmeggiani, L., and Gilardi, F., Med. lavoro, **43,** 179 (1952).

(26) Cadle, R. D., and Johnson, H. S., "Chemical Reactions in Los Angeles Smog", Proc. Second National Air Pollution Symposium, Stanford Research Institute, Los Angeles, Calif. (1952).

(27) Wayne, L. G., and Yost, D. M., J. Chem. Phys., **19,** 41 (1951).

(28) Yost, D. M., and Russel, H., "Systematic Inorganic Chemistry", Prentice-Hall Inc., New York (1944).

(29) Cholak, J., "Proceedings Second National Air Pollution Symposium", p. 6, Pasadena, Calif. (1952).

(30) Katz, M., "Proceedings Second National Air Pollution Symposium, pp. 95-105, Sept. (1952). "Recent Developments in Atmospheric Pollution", CEP-54-23, Am. Gas Assoc. (May 1954).

(31) Morley, M. J., and Tebbens, B. D., Am. Ind. Hyg. Assoc. Quart., **14,** 4 (Dec. 1953).

★ ★ ★